Comet Grains and Implications for Heating and Radial Mixing in the Protoplanetary Disk

Diane Wooden
NASA Ames Research Center

Steve Desch
Arizona State University

David Harker
University of California, San Diego

Hans-Peter Gail
Universitaet Heidelberg

Lindsay Keller
NASA Johnson Space Center

Observations of comets and chondritic porous interplanetary dust particles (CP-IDPs, grains likely shed from comets), as well as of protoplanetary disks, show that a large fraction of the submicron silicate grains in these objects are Mg-rich crystalline silicates. Here we review observations of the mineralogy and crystallinity of cometary grains and anhydrous CP IDPs, including new spectroscopy of the dust liberated by the Deep Impact experiment on 9P/Tempel. Some key results of these observations are: that crystalline silicates are very Mg-rich; and that in most disks (including the Solar System's) a gradient in the silicate crystalline fraction exists. We discuss the mechanisms by which Mg-rich crystals can be produced in protoplanetary disks, including: complete evaporation followed by slow-recondensation; or reduction of Fe in Mg-Fe silicates (possibly facilitated by C combustion to CO or CO_2), combined with thermal annealing. Finally, we discuss how these processes might occur in protoplanetary disks. We conclude that there are three viable scenarios that may operate in protoplanetary disks to produce Mg-rich crystalline silicates with a crystallinity gradient. I) Steady-state conditions can maintain temperatures high enough in the inner disk ($<$ few AU) to evaporate dust and allow it to re-condense; this must be followed by moderately effective outward radial transport of the dust produced. II) Transient heating events, probably shocks, may evaporate dust in the outer disk ($<$ tens of AU) and allow it to recondense over timescales of hours to days, directly producing Mg-rich silicates; alternatively, it may recondense rapidly but be thermally annealed by a second event. III) Transient heating events (shocks) may heat amorphous Mg-Fe silicates only to $\approx$ 1200-1400 K, enough to anneal the dust without destroying it; excess Fe in the silicate must be simultaneously reduced to Fe metal. On the other hand, the presence and characteristics of volatile and refractory organics in cometary materials demonstrate that a significant fraction of the outer disk mass sustained low temperatures ($\sim$30–150 K), and so did not pass through the hottest, inner regions of the disk in the early collapse phase nor was shocked. All models are as yet too incomplete for us to favor any: outward radial transport by turbulent diffusion suffers from a lack of knowledge of the cause of the turbulence; and shock models have not been developed sufficiently to say where in disks shocks can heat or vaporize dust, and for how long. All processes might be simultaneously occurring in disks. What is clear is that cometary grains and anhydrous CP IDPs contain a component of dust – crystalline Mg-rich silicates – that necessarily saw very high temperatures, either by large-scale radial excursions through the solar nebula disk, or by very energetic transient heating events in the comet-forming zone.

1. INTRODUCTION

Data on comets and interplanetary dust particles of probable cometary origin show that amorphous and crystalline silicates were abundant in the protosolar disk. While amorphous silicates are abundant in the interstellar medium (ISM), crystalline silicates are rare. In interstellar clouds in our Galactic disk, amorphous silicates contain magnesium

(Mg) and iron (Fe). In contrast to ISM Mg-Fe amorphous silicates, crystalline silicates in comets and protoplanetary disks are Mg-rich and Fe-poor. In the solar nebula, Mg-rich crystalline silicates formed as the result of high temperature ($\gtrsim$1000 K) processes.

Mg-rich crystalline silicates formed prior to their incorporation into icy cometary nuclei (*Hanner et al.*, 1994). Comet nuclei are the most primitive icy bodies in the solar system, having suffered no post-accretion aqueous or thermal alteration and minimal alteration by cosmic rays and collisions. When perturbed into orbits that pass comet nuclei close to the Sun, nuclear ices, trapped volatile gases, and dust grains are released into a cometary comae. At heliocentric distances of $\sim$1 AU, 0.1 μm silicate grains in cometary comae reach radiative equilibrium temperatures of $\lesssim$400 K (Fig. 1, *Harker et al.*, 2002), insufficient to anneal amorphous silicates. Therefore, Mg-rich crystalline silicates formed in the solar nebula prior to their incorporation into cometary nuclei.

Cometary nuclei also contain materials from the protosolar disk that never saw temperatures above $\sim$30 K – 150 K. For example, in cometary comae the ortho-to-para ratio of H_2O and NH_2 demonstrate that cometary nuclei contain water ice and ammonia ice that last equilibrated at $\sim$30 K (*Kawakita et al.*, 2004b). At sufficiently large heliocentric distances where water ice survives in the coma ($r_h \gtrsim 3$ AU), amorphous water ice has been detected in the near-infrared reflection spectra of comets C/1995 O1 (Hale-Bopp) (*Davies et al.*, 1997) and C/2004 T7 (LINEAR) (*Kawakita et al.*, 2004a). Amorphous water ice has never experienced temperatures above its crystallization temperature of $\sim$150 K.

Cometary nuclei accreted from the colder, icy regions of the solar nebula, beyond the snow line ($\gtrsim$5 AU – 100 AU). The incorporation into cometary nuclei of low temperature materials, e.g., amorphous water ice that never experienced temperatures above 150 K, and high temperature materials, i.e., crystalline silicates, implies that high temperature materials had to be radially transported from hotter regions of the disk to the colder regions, prior to their accretion into cometary nuclei. If transient heating events, such as shocks, occurred and formed crystalline silicates, then there had to be mixing between the shocked and un-shocked regions.

Crystalline silicates are seen in external protoplanetary disk systems, and now are thought to be tracers of thermal processing at high temperatures ($\gtrsim$1000 K) and of radial transport of grains (e.g., *Furlan et al.*, 2005; *Wooden et al.*, 2005). Infrared (IR) spectral features occur with remarkable similarity in comet C/1995 O1 (Hale-Bopp) and in the protoplanetary disk around Herbig Ae/Be star HD 100546 at wavelengths 11.2, 19.5, 23.5, and 33.5 μm (*Bouwman et al.*, 2003), which are attributable to Mg-rich crystalline silicates (*Koike et al.*, 2003; *Chihara et al.*, 2002). Mg-rich crystalline silicates are detected frequently in intermediate mass pre-main sequence Herbig Ae/Be stars (*Bouwman et al.*, 2001) and are present in some low mass pre-main sequence T Tauri stars (*Furlan et al.*, 2005; *Honda et al.*, 2004).

Understanding the formation conditions of Mg-rich crystalline silicates in the protosolar disk sets the context for interpreting Mg-rich crystalline silicate features in external protoplanetary disks. Mg-rich crystalline silicates are present in the most primitive solar system materials – comets, anhydrous chondritic porous (CP) interplanetary dust particles (IDPs) of probable cometary origins, and type 3.0 chondrites (*Brearley*, 1989; *Scott and Krot*, 2005; *Wooden et al.*, 2005). On the other hand, Fe-rich crystalline silicates are abundant in meteoritic materials that have experienced 'secondary formation' mechanisms, such as thermal ($\sim$500 K) and aqueous alteration (*Scott and Krot*, 2005) on asteroidal parent bodies. Therefore, Mg-rich crystalline silicates are 'primary formation' products of thermal processing in the protosolar disk ($\gtrsim$1000 K), by either condensation or annealing. Vaporization of ISM Mg-Fe amorphous silicates followed by condensation thermodynamically favors the formation of Mg-rich crystalline silicates and Fe-metal, thus transforming the reservoir in which the iron resides from within silicates to a separate mineral phase.

Annealing, i.e., the devitrificiation of amorphous silicates into crystalline silicates by heating, does not change the chemical composition (stiochiometry) of the grain: Mg-rich amorphous silicates anneal to Mg-rich crystalline silicates and Fe-rich amorphous silicates anneal to Fe-rich crystalline silicates. The formation of Mg-rich crystalline silicates from the protosolar disk's reservoir of ISM Mg-Fe amorphous silicates by annealing requires a mechanism to metamorphose Mg-Fe silicates into Mg-rich silicates. When Mg-Fe silicates are heated in the presence of elemental carbon (C), the C combusts to CO or CO_2 and FeO in the silicates is reduced to Fe-metal. Reduction of Fe is one 'primary formation' mechanism that may contribute to the viability of the annealing scenario for the formation of Mg-rich crystalline silicates from ISM Mg-Fe amorphous silicates.

The abundance of carbon in CP IDPs is on average $\sim$12 wt-%, which is 2–3 times more than the most primitive CI chondrites (*Thomas et al.*,1994, 1996; *Keller et al.*, 2004). In CP IDPs, carbon takes the forms of amorphous carbon or poorly-graphitized carbon, and organic matter. The carbonaceous matter appears as coatings on single mineral crystals or as the matrix that 'glues' the CP IDP aggregate together.

There is a potential link between the primary thermal processing of silicates and carbonacoues matter in the protosolar disk: C combusts to CO or CO_2, consuming oxygen and driving the reduction of Fe^{2+} in silicates to surface Fe-metal and silica. Surface Fe-metal is an important catalyst for the formation of organic molecules. Heating may transform organic materials to elemental carbon. Comets being more abundant in carbon than CI chondrites suggests that materials in the colder, outer protosolar disk regions probably provided carbon to the inner disk or to regions of shocks for primary thermal processing.

Understanding the origins of cometary materials provides a basis for interpreting silicate crystallinity and mineralogy and carbonceous species in terms of the physical conditions under which dust grain materials formed and aggregated, and were transported in our protosolar disk and in external protoplanetary disks. The properties of silicates and carbonaceous species in cometary comae and in anhydrous CP IDPs are presented in *Section* 2. Plausible formation scenarios for Mg-rich crystalline silicates, including condensation, and annealing combined with Fe reduction are discussed in *Section* 3. Models for protoplanetary disks and for shock-heating in the protosolar disk are presented in the context of crystalline silicate formation scenarios in *Section* 4. Conclusions are presented in *Section* 5.

2. COMET GRAINS AND ANHYDROUS CP IDPs

We utilize a combination of investigative techniques, including remote sensing of cometary comae materials, *in situ* mass spectrometer measurements on flyby spacecraft, and laboratory investigations of anhydrous CP IDPs to assemble the inventory of cometary carbonaceous and siliceous grain materials. Three types of cometary grain materials are presented based on their degree of volatility: the volatile organics, the refractory organics, and the refractory minerals. The volatile organics have such short lifetimes that they are only observable in cometary comae. The refractory organic material survives transit through cometary comae into the interplanetary medium and is present in CP IDPs. Cometary refractory organics may be a mixture of presolar organics and organics formed by 'primary' processes in the early solar nebula. Cometary refractory organic matter constitutes the matrix of anhydrous CP IDPs that 'glues' the refractory minerals together. Cometary refractory minerals are the Mg-Fe amorphous and Mg-rich crystalline silicates, and amorphous carbon detected in cometary comae grains, as well as FeS found in anhydrous CP IDPs, and less abundantly silica (SiO_2) in aggregate GEMS (*Keller et al.*, 2005). The refractory minerals represent relic ISM Mg-Fe amorphous silicates and Mg-rich crystalline silicates that formed in 'primary' thermal processes including condensation and annealing.

To date, the best-studied laboratory samples of the most primitive solar system materials are anhydrous CP IDPs collected in the Earth's stratosphere. Anhydrous CP IDPs are thought to be of cometary origin (*Hanner and Bradley*, 2004; *Wooden*, 2002; *Joswiak et al.*, 1996) because: (a) they contain organic materials with deuterium-to-hydrogen (D/H) isotopic ratios that vary on submicron scales, ranging from sub-solar deuterium (D) ($\lesssim$-400 ‰) to enormous D-enriched materials ($\gtrsim$3000‰) of presolar origin (*Messenger* (2000); *Keller et al.*, 2000); (b) of their relatively high atmospheric entrance velocities ($v \geq 16$km s^{-1}, *Brownlee et al.*, 1995; *Nier and Schlutter*, 1993) that imply they were released from comets on more eccentric orbits than asteroid bodies; (c) they possess anhydrous silicate mineral grains (*Bradley*, 1988); (d) of their highly porous aggregate structures (*Bradley*, 1988); (e) they are unequilibrated aggregates, i.e., aggregates of mineral species that would not exist as adjacent subgrains if heating had occurred after the grains had aggregated; and (f) their refractory mineral subgrains include some of the most primitive materials known in the solar nebula, including GEMS subgrains (Mg-Fe amorphous silicates called Glasses with Embedded Metal and Sulfides), submicron domains of microcrystalline minerals of similar composition called 'equilibrated aggregates', single crystal FeS (*Keller et al.*, 2000), and single crystal silicate minerals with Mg-contents higher than any other solar nebula materials (*Bradley et al.*, 1999b).

Anhydrous CP IDPs are held together by a matrix of organic materials: anhydrous CP IDP subgrains were exposed to either high or low temperatures prior to but not subsequent to grain aggregation. The properties of anhydrous CP IDPs reveals that primary thermal processes and radial transport was happening to submicron-size grain material at the time grains were aggregating, prior to their accretion into cometesimals. Within this next year, laboratory studies of grains collected from the coma of Jupiter Family comet 81P/Wild 2 by the Stardust Comet Sample Return Mission will add significantly to our knowledge of anhydrous CP IDPs.

2.1 Semi-Refractory Organic Grain Species Produce 'Distributed' Sources in Cometary Comae

The greatest alteration to the semi-refractory organic grain species in comets occurs in cometary comae (*Mann et al.*, 2005). In many but not all comets, gaseous species are observed in comae to be more radially extended than the dust (*Bockelée-Morvan et al.*, 2004; *Bockelée-Morvan and Crovisier*, 2002). These radially 'extended' sources of volatile gases are thought to be 'distributed' into cometary comae by dust grains: molecular species are hypothesized to appear in the coma as a result the desorption of an organic grain component(s) after a finite lifetime (typically hours at $\lesssim$ 3-4 AU) (*Bockelée-Morvan and Crovisier*, 2002; *DiSanti et al.*, 2001). The production rates from distributed sources can be similar in magnitude to the production rates of 'native' volatile gases released from the nucleus. To date, the carriers of the distributed sources are a great mystery in cometary science. Different species appear as distributed sources depending on the heliocentric (r_h) distance of the comet. In comet Hale-Bopp, the molecular species that were observed to be 'distributed' were: at 5–14 AU, CO; at 3–5 AU, CO, H_2O, CH_3OH, and H_2CO; at $\lesssim$3 AU, H_2CO, HCN, OCS, and SO, and other species; at $\lesssim$1.5 AU, CO, CN, and C_2. Understanding the carriers of the distributed sources is important to translating comae abundances into nuclear abundances and assessing the solar nebula reservoir out of which comets accreted.

Grain aggregates may fragment in comae when distributed sources are released as the organic materials that serve as the 'glue' that binds aggregates of mineral subgrains together desorbs (*Jessberger et al.*, 2001; *Harker et al.*, 2002). The inner coma of comet 1P/Halley (8900 –

29000 km) had ∼2.4 times the abundance of organic matter (CHON particles) than the outer coma (29000 – 40000 km), according to the Vega 1 flyby mass spectrometer measurements of ∼1 ng of comae cluster grains (*Fomenkova et al.*, 1994). Distributed sources in cometary comae may be the primary tool for investigating the semi-refractory organic grain species extant in the early solar nebula.

2.2 Refractory Organic Materials in Comet Grains and in Anhydrous CP IDPs

One-half of the carbon in anhydrous CP IDPs is in organic materials. The other half of the carbon is elemental C in the form of amorphous carbon or poorly graphitized carbon (*Flynn* et al., 2003; *Thomas et al.*, 1996). On average, anhydrous CP IDPs are ∼6 wt-% amorphous carbon. Given the extreme variability in the C wt-% in an individual anhydrous CP IDP, these laboratory measurements of anhydrous CP IDPs agree well with the amorphous carbon mass fraction of 7– 12 wt-% deduced for comet Hale-Bopp at 0.95–2.8 AU from thermal emission model fits to observed IR spectral energy distributions (*Harker et al.*, 2002, 2004) (*Section* 2.3).

Understanding the composition of cometary organic refractory materials is important because: (1) these materials probably are the precursors of primitive meteoritic organics and by comparison reveal the effects of primary thermal processing on organics, and (2) these materials are the best representative samples of solid-phase organics formed in the ISM (*Keller et al.*, 2004). Cometary refractory organic grain species are best studied with laboratory investigations of anhydrous CP IDPs, *in situ* measurements, and comet sample return missions (Stardust). To date, there is no direct spectroscopic detection of a refractory organic grain species in cometary comae; a 3.4 μm feature seen in a few comets including Halley, C/1989 X1 (Austin), C/1990 K1 (Levy), and the Deep Impact-induced ejecta of comet 9P/Tempel (*A'Hearn et al.*, 2005). The 3.4 μm feature is partly attributable to methanol, with the remainder of the band arising from gas-phase fluorescence and not from refractory organics (*Bockelée-Morvan et al.*, 2004; *Bockelée-Morvan et al.*, 1995). An indirect assessment of the cometary refractory organic grain component comes from models for the observed visible light scattering and polarization of comet comae, which require a highly absorbing organic grain mantle (*Kimura et al.*, 2003).

In the coma of comet Halley, refractory organics were studied *in situ* by the mass spectrometers on Vega-1, Vega-2 and Puma-1, and found to contain primarily C, H, O, and N with a wide variation in relative elemental abundances. Halley's so-called 'CHON' particles were more abundant in the inner coma and constituted ∼25% of the total population of cluster particles, with another ∼25% being CHON-free siliceous particles (*Schulze et al.*, 1997) and 50% being mixtures of CHON and silicecous materials (*Kissel*, 1999). While the majority (∼70%) of the CHON clusters were kerogen-like organic compounds (*Fomenkova*, 1999), a significant minority was elemental carbon (19%) and hydrocarbons (10%) (*Fomenkova et al.*, 1994). The heterogeneity of the chemical properties of the CHON refractory organics is incompatible with their formation in the same protosolar disk environment: Halley's nucleus accreted refractory organic materials that formed in different spatial regions, e.g., the ISM, the prenatal molecular cloud, and the protosolar disk, or experienced different thermal histories (*Fomenkova et al.*, 1994).

In anhydrous CP IDPs, carbonacous material occurs in three different morphologies: (1) as thin (0.01 μm) coatings on single mineral crystals, (2) as discrete submicron- to micron-size domains (carbonaceous units), and (3) as the matrix (∼0.5 μm coatings or domains) that apparently 'glue' subgrains together (*Flynn et al.*, 2003). Individual CP IDPs are found to have a wide range (2–90 wt-%) of carbon abundances (*Thomas et al.*, 1994, 1996; *Flynn et al.*, 2003, 2004; *Keller et al.*, 2004). The average carbon abundance determined for 100 CP IDPs is ∼12 wt-%, which is a factor of 2—3 times more than CI chondrites. For a sample of 19 IDPs, on average 30–50% of the carbon is in organic species with either aliphatic hydrocarbons (1–3 wt-%) or carbonyl (C=O) bonds (∼2 wt-%) (*Flynn et al.*, 2004). In anhydrous CP IDPs the aliphatic hydrocarbon is the carrier of the D-enrichments (*Keller et al.*, 2004). The aliphatic hydrocarbons, i.e., chains of CH_2 bonds with terminal ends of CH_3 groups, have approximately the same mean aliphatic chain lengths in anhydrous CP IDPs and hydrous CP IDPs, but are longer than in the Murchison CI chondrite (*Flynn et al.*, 2003). Analyses of 3 anhydrous CP IDPs suggests that the organic matter is more complicated (containing two C=O groups) than in hydrous CP IDPs and the Orgueil CI meteorite (*Flynn et al.*, 2004).

The large variations in the D- and ^{15}N-enrichments in the matrices of anhydrous CP IDPs indicates that the organic materials have experienced various degrees of thermal processing and are a mixture of protosolar disk and presolar materials (*Keller et al.*, 2004). On submicron size scales, D-enrichments range from subchondritic (-400 ‰) to strongly enriched ($\gtrsim +10{,}000$) (*Keller et al.*, 2004; *Messenger et al.*, 1996). In one anhydrous CP IDP fragment, high $^{15}N/^{14}N$ isotopic ratios occur in a more refractory phase than the D-rich material, perhaps bonded to the relatively rare aromatic hydrocarbons (*Keller et al.*, 2004). The differences between the anhydrous CP IDP organics and organics in primitive carbonceous meteorites (e.g., *Kerridge*, 1999) indicates that thermal processing: (a) converts aliphatic hydrocarbons from longer to shorter chains; (b) converts alphatic bonds to aromatic bonds; (c) alters the organic material with C=O bonds (*Flynn et al.*, 2003).

2.3 Silicate Mineralogy and Amorphousness *versus* Crystallinity in Comets and in Anhydrous CP IDPs

IR spectra of comet comae, laboratory studies of anhydrous CP IDPs, and *in situ* measurements of Halley's coma all indicate that the predominant refractory minerals are amorphous carbon (also discussed in *Section* 2.2) and silicates with compositions similar to olivine,

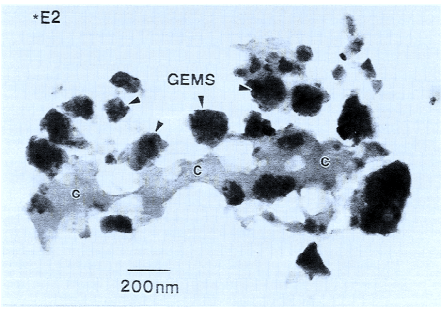

Fig. 1.— GEMS with D-rich amorphous carbonaceous material (C) in an anhydrous CP IDP (L2009*E2) [Fig. 3 of *Keller et al.*, 2000.]

(Mg_y,$Fe_{(1-y)}$)$_2SiO_4$, and pyroxene, (Mg_x,$Fe_{(1-x)}$)SiO_3. Specifically, olivines can be considered as solid solutions of Mg_2SiO_4 (y=1) and Fe_2SiO_4 (y=0), respectively named forsterite (Fo100) and fayalite (Fo0). In the nomenclature of mineralogists, olivine is crystalline, and Fo100–Fo92 is 'forsterite' (*Henning et al.*, 2005). Olivine crystals in cometary materials, however, have higher Mg-contents (Fo98) than in any other solar system materials (*Bradley et al.*, 1999b). Because of this distinction, we will denote Mg-rich for $1.0 \geq y \geq 0.9$ and Mg-Fe for $y \approx 0.5$, and in certain cases, we will use the corresponding notation Fo100–Fo90 and Fo50. Correspondingly, pyroxenes range from pure-Mg enstatite (x=1) to pure-Fe ferrosilite (x=0), denoted En100 and En50, respectively.

By comparison with laboratory minerals, the predominant 9.7 μm silicate feature in comets is attributed to Mg-Fe amorphous olivine, and the short wavelength rise on the feature is attributed to Mg-Fe amorphous pyroxene (*Hanner et al.*, 1994; *Wooden et al.*, 1999; *Wooden*, 2002; *Harker et al.*, 2002, 2004; *Hanner and Bradley*, 2004; *Wooden et al.*, 2005). In amorphous olivine and pyroxene, the vibrational stretching and bending modes of the Si–O bonds produce the 10 μm and 20 μm features, respectively. At any single comet observation epoch, all coma grains are at the same heliocentric distance and the IR emission from the coma is optically thin, so the observed flux density, especially the ratio of the 10 μm/20 μm features, constrains the grain temperatures. Radiative equilibrium grain temperatures (T_{dust}) are strongly dependent on the absorptivity (Q_{abs}) of sunlight at visible and near-IR wavelengths (Fig. 4), and weakly dependent on grain radius ($T_{dust} \propto a^{1/5}$), so grain temperatures probe the optical properties of the grains. From their grain temperatures, cometary amorphous silicates are deduced to have $0.5 \leq x \simeq y \leq 0.7$ (*Harker et al.*, 2002), i.e., they have approximately chondritic (x=y=0.5) Mg- and Fe-contents.

Most cometary silicate features are more 'flat-topped' than amorphous silicate features (*Colangeli et al.*, 1995): IR spectroscopy first detected the 11.2 μm crystalline olivine feature in comet 1P/Halley (*Campins and Ryan*, 1987). The resonant features from crystalline silicates are narrower than features from amorphous silicates. Strong far-IR features at 19.5, 23.5, and 33.5 μm, and weaker features at 16 and 27.5 μm, from Mg-rich crystalline olivine (Mg_y,$Fe_{(1-y)}$)$_2SiO_4$ with $y \geq 0.9$ were detected first in the ISO SWS spectra of comet Hale-Bopp at 2.8 AU pre-perihelion (Fig. 3), providing irrefutable confirmation of the identification of the 11.2 and 10.0 μm features with Mg-rich crystalline olivine (*Crovisier et al.*, 1997). The mineralogical decomposition of 10 μm silicate feature of comet Hale-Bopp is demonstrated in Fig. 2. Features from Mg-rich crystalline pyroxene (Mg_x,$Fe_{(1-x)}$)SiO_3 with $x \geq 0.9$ were detected at 9.3 and 10.5 μm in ground-based mid-IR spectra of Hale-Bopp at 0.93 AU, when the comet was close to perihelion (*Wooden et al.*, 1999; *Harker et al.*, 2002, 2004). The wavelengths of the features observed

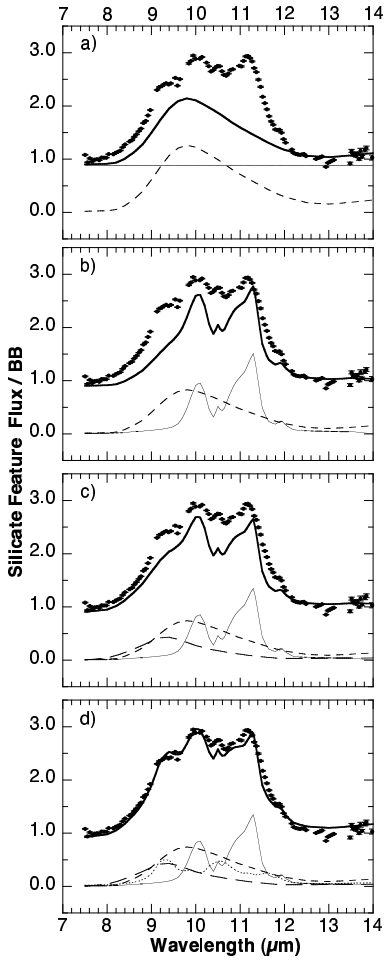

Fig. 2.— The 10 μm silicate feature of comet Hale-Bopp at 0.93 AU on 1997 April 10 UT, shown as the flux divided by a blackbody (BB) fitted to the $\lambda \leq 8.4$ and $\lambda \geq 12.4$ μm emission, is compared with the progressive addition of: (a) amorphous carbon (*light solid* line) and Mg-Fe amorphous olivine (Fo50) (*short dash*); (b) Mg-rich crystalline olivine (Fo90) (*solid*); (c) Mg-Fe amorphous pyroxene (En50) (*long dash*); (d) Mg-rich crystalline orthopyroxene (Fo90) (*dotted*). [*cf.*, Fig. 6, *Wooden et al.*, 1999.]

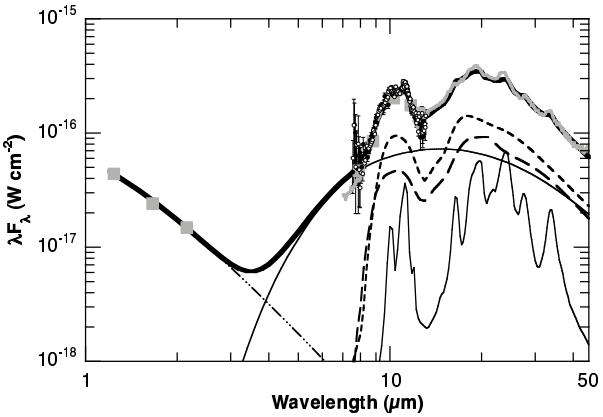

Fig. 3.— SED (λF_λ *versus* λ) of ground-based photometry (*squares*) and spectra (*circles*), and *ISO SWS* (*thick gray line*) data of comet Hale-Bopp at 2.8 AU plotted with the best-fit thermal emission model (*heavy line*). SED is the sum of scattered sunlight ($\leq$ 5 μm) and thermal emission ($\geq$ 3 μm) from a size distribution (slope $= -3.4$, peak grain radius a_p=0.2 μm (*Hanner*, 1983), 0.1 μm$\leq a \leq$ 100 μm) of discrete mineral grains: porous grains of amorphous carbon (*solid*), amorphous Mg-Fe olivine (Fo50) (*short-dash*), amorphous Mg-Fe pyroxene (En50) (*long-dash*), and 0.1–1 μm solid crystalline Mg-rich olivine (Fo90) (*solid*). [Adapted from *Harker et al.*, 2002, 2004.]

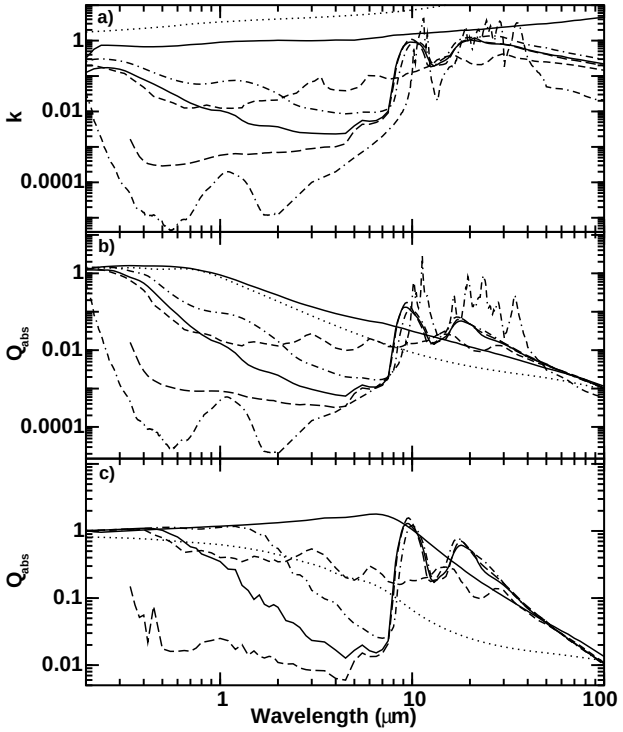

Fig. 4.— Optical properties of minerals given by (a) the imaginary index of refraction, k, and by grain absorptivities ($Q_{abs}(\lambda)$) for grains of (b) 0.1 μm-radii and (c) 1 μm-radii. From the most absorptive to least absorptive minerals (*top to bottom* at 1 μm): iron (dotted); amorphous carbon (solid line); Mg-Fe amorphous olivine [Fo50] (dash-dot); kerogen type II organic (short-dash) (*Khare et al.*, 1990); Mg-Fe amorphous pyroxene [En50] (solid line); Mg-rich amorphous pyroxene [En95] (long-dash); and Mg-rich crystalline olivine [Fo100] (dash-dash- dot). [From *Wooden et al.*, 2005.]

in comets are consistent with high Mg-content crystals, (0.9$\leq x \simeq y \leq$1.0) (*Koike et al.*, 2003; *Chihara et al.*, 2002). In comets, the Mg-content of the crystalline silicates is significantly greater than in the amorphous silicates.

The relative abundances of refractory mineral grains are derived by χ^2-fitting thermal emission models to observed spectral energy distributions (SEDs) (*Harker et al.*, 2002, 2004; Wooden *et al.*, 2004). The best-fit thermai emission model for comet Hale-Bopp at 2.8 AU is shown in Fig. 3. The derived relative abundances depend on the relative grain temperatures, which depend on the mineralogy and Mg-contents. Mg-rich crystals are more transparent at optical and near-IR wavelengths than Mg-Fe amorphous silicates, which are more transparent than amorphous carbon and Fe-metal grains (Fig.4). A Mg-rich crystal absorbs sunlight less efficiently than a Mg-Fe amorphous silicate of the same grain radius (a), so a Mg-rich crystal has a lower radiative equilibrium temperature and emits less flux ($F_\lambda = \pi a^2\, \pi B_\lambda(T_{dust}) Q_\lambda(a)$). A Mg-rich crystal is harder to detect than a warmer Mg-Fe amorphous silicate grain of the same size. Therefore, the silicate crystalline fraction f_{cryst}, i.e., the mass ratio of submicron Mg-rich crystals to the sum of submicron amorphous and crystalline silicates, needs to be greater than $\sim$0.5 for Mg-rich crystals to be detected (in IR spectra with a spectral resolution of $R \sim$100 and signal-to-noise ratio of $\sim$100).

Relatively high crystalline mass fractions are deduced for the submicron portion of the grain size distribution in Oort cloud comets: for Hale-Bopp, $f_{cryst}\simeq$0.6–0.8 (*Harker et al.*, 2002, 2004) and for C/2001 Q4 (NEAT) $f_{cryst}\simeq$0.7 (*Wooden et al.*, 2004); for Hale-Bopp, f_{cryst}=0.79, 0.67, and 0.60 in Figs. 2, 5, and 3, respectively. In contrast, the crystalline mass fraction ($f_{cryst}\simeq$0.35) deduced for the subsurface layers of the nucleus of Jupiter Family comet 9P/Tempel, which were ejected when the Deep Impact Mission hit the comet (Fig. 5; *Harker et al.*, 2005), is lower than for Oort cloud comets. Oort cloud comets and Jupiter Family comets were ejected from the trans-Jupiter and trans-Neptune regions of our protoplanetary disk out to the Oort cloud and Kuiper Belt, respectively (*Gomes*, 2003; *Morbidelli and Levison*, 2003). Comparing f_{cryst} for Oort cloud and Jupiter Family comets implies a radial-dependence to f_{cryst} possibly existed in the protosolar disk (*Harker et al.*, 2005b).

Submicron solid crystals produce the shapes of the observed IR resonances, so the ratio of the mass of submicron crystals to the total mass of submicron silicates defines the crystalline fraction (*Harker et al.*, 2002). Nevertheless, a size distribution of grains that includes larger

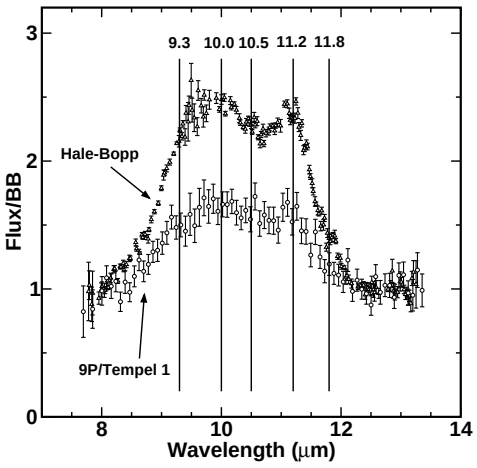

Fig. 5.— Crystalline silicate features in the 10 μm spectra of Oort cloud comet Hale-Bopp (*top*, 1.7 AU post-perihelion) and in the Deep Impact-induced ejecta of Jupiter Family comet 9P/Tempel (*bottom*, 1.5 AU, 1 hr after impact). [Fig. 2 of *Harker et al.*, 2005b.]

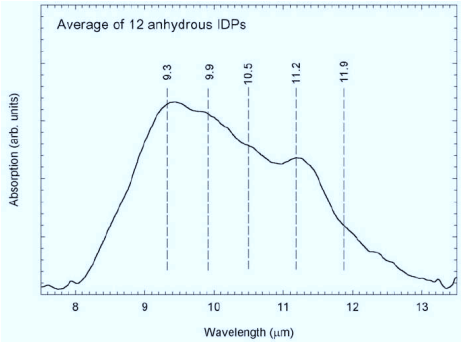

Fig. 6.— Average absorption spectra of 12 anhydrous IDPs. [Fig. 2 of *Keller and Flynn*, 2003.]

(10–100 μm-radii) amorphous silicates contributes to the observed SEDs. If we try to mimic grain aggregates with a grain size distribution that contains submicron crystals as well as submicron- to 100 μm-radii amorphous silicate grains, we may underestimate the crystalline fraction. In fact, crystals may be effectively spectroscopically hidden within larger aggregates: IR spectral features of anhydrous CP IDP thin sections reveal resonances of stronger contrast than bulk particles (*Molster et al.*, 2001; *Bradley et al.*, 1999c). Given these caveats, taking a grain size distribution into account out to 10 μm-radii, rather than just the 0.1–1 μm grains, yields lower crystalline mass fractions: $f_{cryst} \simeq 0.4$ for Hale-Bopp, and $f_{cryst} \simeq 0.2$ for 9P/Tempel that is still higher than $f_{cryst} \lesssim 0.02$ deduced for any other Jupiter Family comet (*Sugita et al.*, 2005). A significantly lower crystalline mass fraction of $f_{cryst} \simeq 0.075$ is derived for Hale-Bopp using a grain size distribution with submicron crystals, submicron to $\sim$100 μm-radii amorphous minerals, and non-spherical particle shapes (*Min et al.*, 2005a).

In-situ mass spectrometer measurements of Halley do not reveal the amorphousness or crystalliniity of the comae grains (*Kissel*, 1999), but do yield the relative mass fractions of elements (Mg, Si, S, Fe), whose relative ratios reveal the possible minerals present. Given (Mg+Fe):Si $\simeq$1 for pyroxene and 2 for olivine, the mass spectrometer measurements (Table 2 of *Schulze et al.*, 1997; *Schulze and Kissel*, 1992) indicate that the dominant ($\gtrsim$50% by mass) refractory mineral is Mg-rich pyroxene ($0.8 \gtrsim$ x $\gtrsim 0.9$). Also present are significant mass fractions ($\sim$25%) of Mg-Fe olivine (y$\simeq$ 0.5) and smaller mass fractions of pure-Mg olivine ($\sim$5%), FeS ($\sim$10%) and Fe-metal grains ($\sim$3%) (*Schulze et al.*, 1997). Most (70%) of the iron is in Fe or FeS grains, with the remaining fraction (30%) being in siliceous grains; some siliceous grains also contain S. The Mg-Fe olivine in Halley may be the Mg-Fe amorphous silicates detected in IR spectra of comets.

Anhydrous CP IDPs are important comparison materials for fine-tuning our understanding of the refractory minerals in cometary dust. The dominant refractory mineral phases in anhydrous CP IDPs are Mg-rich crystalline silicates, GEMS (*Section* 2; *Bradley et al.*, 1999c), Fe-sulfides (*Keller et al.*, 2000), and amorphous or poorly graphitized carbon. Submicron and micron-size single crystals of Mg-rich pyroxene and olivine can constitute 20–30% of mass of a anhydrous CP IDP. For example, IDP L2009*E2 (Fig. 1) has 5–10% by mass Mg-rich crystalline silicates.

IR spectra of the major mineral phases in anhydrous CP IDPs have features at the same wavelengths as the IR spectra of comets (*Bradley et al.*, 1992; *Wooden et al.*, 2000; *Bradley et al.*, 1999a, c; *Keller and Flynn*, 2003). The 10 μm absorption spectrum derived from the average of 12 anhydrous CP IDPs (Fig. 6) has features at the same wavelengths in the 10 μm emission spectrum of comets Hale-Bopp and 9P/Tempel (Fig. 5). Crystalline olivine and pyroxene are more Mg-rich than in other primitive solar system laboratory samples (carbonaceous chondrites, Antarctic micrometeorites) (*Bradley et al.*, 1999b). The wavelength positions of the far-IR spectral resonances in one anhydrous CP IDP thin section (Fig. 7), however, reveal a domain of microcrystalline olivine of Fo75 that is less Fo90–100 deduced for crystalline olivine in comet Hale-Bopp.

In anhydrous CP IDPs, iron is contained in macroscopic (micron-sized) FeS crystals and nano-phase Fe and FeS in GEMS. S is concentrated in Fe-sulfides (*Flynn et al.*, 2004). FeS is most frequently observed toward the outer surfaces of GEMS than the centers. This gradient may be a consequence of S diffusion into the GEMS, while in the solar nebula (*Keller*, private communication).

When detailed laboratory studies of dozens of individual anhydrous CP IDPs are compared to the properties of comae grains deduced from IR spectroscopy alone, we find that anhydrous CP IDPs are similar to comae grains in that they contain: (a) Mg-Fe amorphous silicates and GEMS, respectively; (b) Mg-rich crystalline olivine and Mg-rich crystalline orthopyroxene; and (c) amorphous carbon. At the same time, anhydrous CP IDPs are different in that

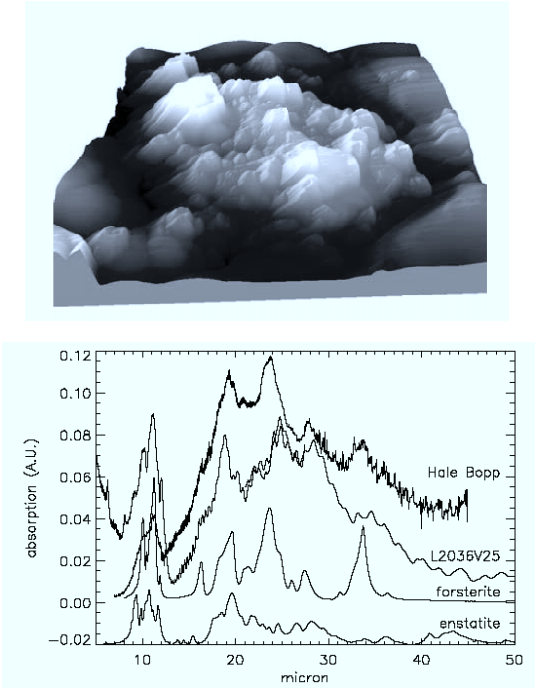

Fig. 7.— (*Top*) Atomic Force Microscope image of Mg-rich crystals within thin-section of anhydrous CP IDP L2036V25 (10 μm$\times$10 μm$\times$3 μm). (*Bottom*) 5–50 μm transmission spectrum of IDP L2036V25 thin-section compared to pure-Mg crystalline olivine (forsterite) and pyroxene (enstatite), and to the emission spectrum of comet Hale-Bopp (*Crovisier et al.*, 1997). The Mg-content of the olivine (Mg_y,$Fe_{(1-y)}$)$_2SiO_4$ crystals in Hale-Bopp ($y \geq$0.9) are higher than in this IDP ($y \geq$0.75), based on the wavelengths of the far-IR features. [From *Molster et al.*, 2003.]

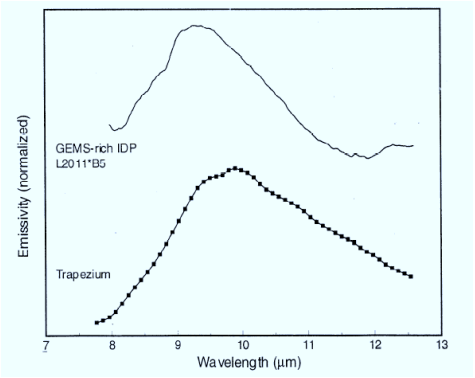

Fig. 8.— The 10 μm feature of a GEMS-rich section of an anhydrous CP IDP is broad (*Bradley et al.*, 1999], characteristic of amorphous silicates, and is compared to the ISM feature towards the Trapezium. [From *Keller et al.*, 2000.]

they contain: (d) more enstatite than forsterite (*Keller et al.*, 2004; *Keller and Flynn*, 2003); (e) a matrix composed of not only amorphous carbon but also refractory organics that are not detected spectroscopically; (f) domains of Mg-rich crystalline olivine with lower Mg-contents compared to that deduced from IR spectra (far-IR comparison in Fig. 7); and (g) FeS single crystals (*Keller et al.*, 2000). *In situ* measurements of a ng of mass of comae grains are in concurrence with studies of anhydrous CP IDPs in that they contain: (d), (e), and (g), while (f) is not determinable from mass spectrometer measurements. It is important to note than pure-Mg amorphous silicates as well as discrete Fe-rich crystalline silicates are absent from anhydrous CP IDPs. In summary, IR spectra do not reveal the presence of Fe or FeS grains nor detect the refractory organic grain component that are seen in anhydrous CP IDPs and *in situ* measurements of comet comae.

2.4 Mg-Fe Amorphous Silicates are Interstellar

Along lines-of-sight through the ISM, silicate absorption features are well-matched by Mg-Fe amorphous olivine and pyroxene (*Kemper et al.*, 2004, 2005). Mg-rich crystalline silicates are rare (<5%, *Li and Draine*, 2001) to absent ($\leq$ 1.1 $\pm$ 1.1% towards the Galactic Center, *Kemper et al.*, 2004, 2005). Detailed analysis of the ISM extinction curve implies the presence of Mg-Fe amorphous silicates (*Li and Draine*, 2001). Studies of the depletion of gas-phase atoms into dust grains in Galactic diffuse ISM clouds show Fe, Mg, and Si are depleted together in grains, and in increasing amounts for denser clouds (*Jones*, 2000; *Savage and Sembach*, 1996). Through depletion studies, a less-refractory dust phase that contains Mg and Si and no Fe is seen to exist in clouds in the Galactic halo above the Galactic disk (*Jones*, 2000). The ISM silicate absorption feature towards the Galactic center can be fitted by non-spherical amorphous pure-Mg silicates as well as by spherical Mg-Fe amorphous silicates (*Min et al.*, 2005b), demonstrating that particle shape can affect the shape of the resonances and the interpretation of the mineralogy and Mg- and Fe-contents. However, the depletion studies taken together with models for the shape of the 10 μm absorption feature imply that Galactic disk ISM silicates are Mg-Fe amorphous olivine and pyroxene.

Mg-Fe amorphous silicates are deduced to be dominant components of comet comae grain populations (*Section* 2.3), and are present in anhydrous CP IDPs as GEMS or Glasses with Embedded Metal and Sulfides (*Bradley et al.*, 1999c; *Flynn et al.*, 2003). GEMS are not well-defined stoichiometric olivines and pyroxenes, but have elemental ratios suggesting a mixture of compositions spanning olivine and pyroxene compositions (*Bradley et al.*, 1992; *Brownlee et al.*, 1999; *Keller and Messenger*, 2004a). The absorption feature from GEMS-rich anhydrous CP IDP material has a similar shape as the ISM absorption feature (Fig. 8; *Bradley*, 1994a, b). For more than a decade, GEMS have been considered as the prototypical ISM Mg-Fe amorphous silicate (*Hanner and Bradley*, 2004).

A recent hypothesis that 80–90% of GEMS are 'non-equilibrium condensates that have escaped annealing and further reaction with the gas phase (except for late sulfidiza-

tion of Fe)', *which formed in the solar system* (*Keller and Messenger*, 2004a, b); *Keller et al.*, 2005) implies a similar mass of more volatile ISM organics and ices would have been subjected to high temperatures in the protosolar disk. However, the large abundance of ISM volatile gases and ices (*Bockelée-Morvan et al.*, 2000; *Ehrenfreund and Charnley*, 2000; *Ehrenfreund et al.*, 2004) and organics (*Keller et al.*, 2003) in cometary materials refutes this concept.

An argument used to substantiate the solar system origin for both GEMS and Mg-rich crystalline silicates is that ∼99% of the mass of more than 1000 subgrains of anhydrous CP IDPs have homogeneous solar isotopic ratios of $^{17}O/^{16}O$, $^{18}O/^{16}O$, and $^{15}N/^{14}N$ (*Messenger*, 2000; *Messenger et al.*, 2003). Nevertheless, grains could lose the isotopic signatures of their sites of origin in AGB stars, novae, and supernovae if re-formed in ISM clouds after being sputtered or destroyed by shocks (*Jones*, 2000). To date, there is no consensus as to whether the isotopic homogeneities in subgrains in anhydrous CP IDPs can be interpreted as evidence for their formation in the protosolar disk or for grain homogenization in the ISM (see *Tielens*, 2003).

Sources for ISM Mg-Fe amorphous silicates include O-rich Asymptotic Giant Branch (AGB) stars and supernovae. AGB stars primarily shed Mg-Fe amorphous silicates, but up to 4–20% of their siliceous grains may be Mg-rich crystalline silicates (*Kemper et al.*, 2001). Crystalline silicates dispersed via stellar winds into the ISM, however, probably are rapidly amorphized by the bombardment by cosmic rays. Bombardment by low energy Galactic cosmic rays (few–50 keV H^+ or He^+ ions) probably efficiently amorphizes crystalline silicates (*Carrez et al.*, 2002; *Jäger et al.*, 2003; *Brucato et al.*, 2004; *Bradley*, 1994a; *Dukes et al.*, 1999), with chemical composition alteration occurring at $\lesssim$20 keV (*Carrez et al.*, 2002; *Bradley*, 1994a). Also, low energy (4–10 keV) cosmic-ray exposure can reduce iron from its stioichiometric inclusion in an amorphous Mg-Fe silicate mineral grain to nano-phase Fe metal embedded within the Mg-rich amorphous silicate grain (*Carrez et al.*, 2002), such as seen in GEMS (*Bradley*, 1994a). Amorphization by high energy, heavy cosmic rays (1.5 MeV Kr^+ ions) occurs at one-quarter the dose for Fe-rich crystalline olivine (Fe_2SiO_4) than for Mg-rich crystalline olivine ($Mg_{0.88}$,$Fe_{0.12}$)$_2SiO_4$, and the distances from supernovae shocks traveled by MeV cosmic rays (∼2 pc, *Spitzer and Jenkins*, 1975) are greater than for KeV cosmic rays, so preferential amorphization of Fe-bearing crystalline silicates in the ISM may explain the preponderance of Fe-bearing amorphous silicates in astrophysical objects including comets, AGB stars, and post-AGB environments (*Jäger et al.*, 2003).

3. FORMING MG-RICH CRYSTALS IN DISKS

In protoplanetary disks, some fraction of the initial reservoir of interstellar Mg-Fe amorphous silicate grains accreted into the outer regions from the prenatal cloud core are converted into the Mg-rich silicate crystals. The processes that form pure-Mg or Mg-rich crystals are: (I) vaporization followed by gas-phase condensation of solids under conditions that favor thermodynamically stable pure-Mg crystalline silicate minerals in chemical equilibrium; (II) vaporization followed by rapid nucleation and growth of amorphous Mg-rich silicates under kinetically controlled conditions, followed by annealing; and (III) annealing of Mg-Fe amorphous silicates (formed by rapid condensation or interstellar in origin) into crystalline Mg-Fe silicates coupled with reduction of Fe out of the grains under the typical reducing (as opposed to oxidizing) conditions in the solar nebula gas. Since neither Mg-rich amorphous silicates nor Mg-Fe crystalline silicates are a substantial component of cometary comae or anhydrous CP IDPs, so scenarios (II) and (III) imply ∼100% efficiency.

3.1 Condensation from Nebular Gases

Mg-rich crystalline silicates are thermodynamically favored to condense in hot, dense inner disks. When partial pressures of condensible materials are high enough that kinetic barriers are overcome, often under conditions of 'supersaturation', molecular species nucleate into molecular clusters and cluster growth ensues (e.g., *Colangeli et al.*, 2003). Rapid growth produces highly disordered particles (*Nuth et al.*, 2002; *Rietmeijer et al.*, 2002). If temperatures are high enough, clusters rearrange themselves into regular structures or crystals (*Colangeli et al.*, 2003), or clusters grow 'epitaxially' as crystals on pre-existing crystalline 'seed' grains. Growth of single crystals from nebular gases can explain the relatively infrequent (*Bradley*, private communication) platelet or ribbon forms of forsterite and enstatite crystals in anhydrous CP IDPs (*Bradley et al.*, 1983; *Scott and Krot*, 2005; see Fig. 2 in *Keller et al.*, 2000).

In protoplanetary disk environments where there are sustained high partial pressures of refractory elements (*Grossman*, 1972; *Pataev and Wood*, 2005), such as in the midplanes of inner disks, a high proportion of crystalline minerals are expected to be produced. The dominant mineral phases to condense as the gas cools are (Fig. 9; *Gail*, 2003): first, oxides, e.g., corundum or Al_2O_3; second, Mg-rich crystalline silicates, i.e., forsterite (Mg_2SiO_4), and enstatite ($MgSiO_3$), and Fe-metal; third, at much cooler temperatures, troilite or FeS.

In chemical equilbrium models, orthoenstatite is predicted to be the dominant silicate condensate (e.g., *Grossman*, 1972; *Petaev and Wood*, 1998). The conversion of forsterite into enstatite is governed by the diffusion of cations and occurs on fairly long time scales compared to disk evolution time scales: a 0.1 μm radii forsterite crystal is converted into an enstatite crystal in 10^6 yr at ∼1350 K (*Gail*, 2004). During 10^6 yr, protoplanetary disk midplanes cool as their mass accretion rates decline (*Wehrstedt and Gail*, 2002; *Keller and Gail*, 2004), so the relatively slow forsterite-enstatite conversion probably does not attain chemical equilibrium at all times throughout the protosolar disk. The forsterite-to-enstatite ratio is diverse in primitive

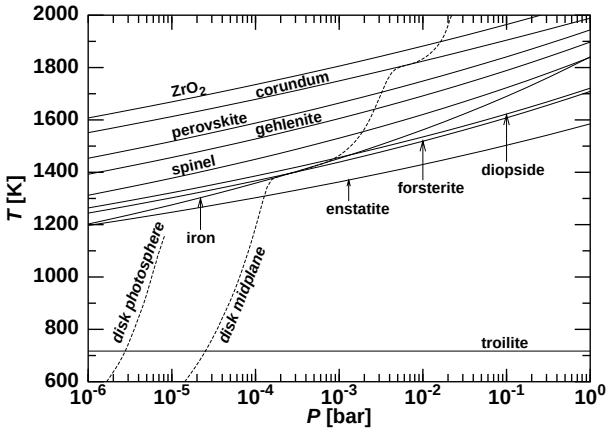

Fig. 9.— The stability limits of the important solid phases in the pressure regime of interest for accretion discs. Also shown are the typical P-T-combinations in the midplane of the disk and in the disk atmosphere. As the gas cools in the mid-plane, at P$> 10^{-3}$ [bar] Fe-metal grains condense out before forsterite (Mg_2SiO_4) and enstatite ($MgSiO_3$).

chondrite matrices (*Scott and Krott*, 2005); appears high based on IR spectroscopy of comet comae (Fig. 2) but low based on Halley fly-by measurements; and is high in anhydrous CP IDPs for the domains of polycrystalline 'equilibrated aggregates' (Fig. 7) but low for the larger ($\sim$0.5–5 μm) single crystals (see Fig. 2 of *Keller et al.*, 2000). A larger sample of high signal-to-noise comet IR spectra as well as analyses of Stardust Mission returned samples will provide further constraints on the degree of forsterite-enstatite conversion in the protosolar disk.

3.2 Condensation of Amorphous Silicates

The conditions for equilibrium cannot be expected to persist throughout the disk, as transient heating events such as shocks are likely to occur. A higher proportion of amorphous silicates relative to crystalline silicates are expected to be produced in environments characterized by low partial pressures of condensable elements and rapid cooling, e.g., in stellar outflows (*Molster and Kemper*, 2005), and possibly in X-winds (*Shu et al.*, 2001), protostellar winds (*Kenyon et al.*, 1991), and shocks that melt grains (*Desch and Connolly*, 2002). In regions where low partial pressures of condensable elements exist, condensation will be controlled largely by kinetics, and not by thermodynamics (*Gail and Sedlmayr*, 1999; *Gail*, 2004). Rapid growth of more highly disordered clusters will ensue when gas temperatures drop and supersaturation occurs.

Experiments of vapor-phase condensation from mixtures of gases at $\sim$1000 K form highly disordered 'smokes' or fine-grained films of magnesiosilica ($MgO.SiO_2$) or ferrosilica (Fe_2O_3 + SiO_2) compositions but not Mg-Fe silicates (*Hallenbeck et al.*, 1998; *Rietmeijer*, 1998; *Rietmeijer et al.*, 2002; *Nuth et al.*, 2002). Rapid condensation scenarios for amorphous silicates in the chondrule-forming region are discussed by *Nuth et al.* (2005). In addition, amorphous silicate minerals are formed by rapid quenching ($\sim$2000 °C/sec) of a melt (*Dorschner et al.*, 1995), by gel-dissication (chemical reactions forming a gelatinous precipitate) (*Thompson et al.*, 2002, 2003), or by vaporizing crystalline silicate mineral samples at $\sim$5000 K with a pulsed laser (*Brucato et al.*, 2002; *Fabian et al.*, 2000; *Brucato et al.*, 1999). Amorphous enstatite prepared by gel desiccation have Si–O tetrahedonal 'proto-forsteritic' structures (*Thompson et al.*, 2002, 2003). Amorphous silicate condensates formed by laser ablation, including forsterite, fayalite (Fe_2SiO_4), enstatite, and silica (SiO_2), appear to have more homogeneous mineral compositions than vapor-phase amorphous condensates, possibly because at higher temperatures congruent evaporation of molecular clusters yields condensates with compositions similar to the starting minerals, whereas vapor-phase condensates must nucleate clusters from the gas (*Brucato*, private communication; *Nuth*, private communication).

3.3 Annealing of Amorphous Silicates

Amorphous silicates are prepared for laboratory annealing experiments using three different processes: vapor condensation, laser ablation, and gel desiccation (*Section* 3.2). Sample preparation techniques impact the composition and structures of amorphous silicate materials and the temperatures and durations of heating required to anneal these samples (see *Wooden et al.*, 2005 for a detailed review).

Despite the differences between the chemical compositions and structures of the amorphous silicate samples prepared by different laboratory techniques, the experiments to anneal amorphous silicates into crystalline silicates come to some general conclusions: (1) The stiochiometry or chemical composition of the starting amorphous material is not altered by annealing, but rather revealed by annealing; Mg-rich amorphous silicates anneal to Mg-rich crystals, Fe-rich amorphous silicates anneal to Fe-rich crystals, Mg-Fe amorphous silicates anneal to moderately Fe-rich crystals and proto-forsteritic structures in amorphous enstatite samples prepared by gel desiccation anneal to forsterite. [Amorphous oxide mixtures ($MgO–SiO_2–Fe_2O_3$) prepared by laser ablation and then annealed at 1000 K for 1 hr have mid-IR resonant features at the same wavelengths as annealed forsterite, but far-IR features at slightly ($\sim$0.1–0.3 μm) different wavelengths (*Brucato et al.*, 2002). This experiment has not been repeated.] (2) Amorphous magnesiosilica materials anneal at lower temperatures than amorphous ferromagnesia materials (*Hallenbeck et al.*, 1998; *Brucato et al.*, 2002; *Nuth et al.*, 2005). (3) At $\sim$1100–1000 K, Mg-rich amorphous pyroxenes complete annealing in $\sim$1–4 hr, with the exception of vapor-condensed samples that may take up to $\sim$200 hr. (4) At $\sim$1100–1000 K, Mg-rich amorphous olivines complete their annealing in $\sim$4–12 hr or longer (see Table 1, *Wooden et al.*, 2005 for a summary of activation energies). (5) Mg-rich crystalline silicate resonances arise from micro-crystalline structures as well as from crystallized 0.1 μm spherules (*Brucato et al.*, 1999).

(7) Domains of long-range order still may exist within amorphous silicates, even though IR spectroscopy nor X-ray diffraction can detect periodic structures of crystalline materials in laboratory-prepared amorphous silicates (e.g., *Colangeli et al.*, 2003). Such domains can act as nucleation sites that promote crystallization more rapidly or at lower annealing temperatures (*Thompson et al.*, 2003; *Colangeli et al.*, 2003; *Brucato et al.*, 2002). (8) The most highly disordered vapor-phase condensates take the longest to anneal, with a 'stall' (*Hallenbeck et al.*, 1998) that may be analogous to rearragement into congruent molecular clusters that exist apriori in amorphous silicates prepared by laser ablation (*Rietmeijer et al.*, 2002). Hence, the most conservative approach to computing annealing times is to use the Silicate Evolution Index (SEI) (*Hallenbeck et al.*, 2000) that characterizes the annealing times of the most disordered amorphous silicate samples, i.e., the vapor-phase condensates (*Rietmeijer et al.*, 2002).

Fe-rich amorphous silicates and Fe-rich crystalline silicates are not identified in the IR spectra of comets, are not abundant in anhydrous CP IDPs, and are not inferred to exist from *in situ* measurements of Halley, so the condensation and annealing of Fe-rich amorphous silicate phases appears to play an insignificant role in primary thermal processing in the protosolar disk. Even so, it is interesting to note that Fe-rich amorphous silicates anneal at such high temperatures that partial vaporization may occur, lessening the resultant radii of Fe-rich crystals (*Nuth and Johnson*, 2006).

Mg-rich amorphous silicates are not an abundant component of anhydrous CP IDPs, nor are they deduced to dominate cometary comae (i.e., comet Hale-Bopp, *Harker et al.*, 2002). If the chemically-favored formation of pure-Mg amorphous silicates by rapid condensation occurred in the protosolar disk (Fig. 11), then these Mg-rich amorphous silicates were annealed to Mg-rich crystalline silicates at $\gtrsim$1000 K with nearly 100% efficiency.

Heating GEMS, the Mg-Fe amorphous silicates in anhydrous CP IDPs, produces moderately Fe- rich (Mg-Fe) olivine crystals through a subsolidis devitrification (*Brownlee et al.*, 2005). The absence of Mg-Fe crystalline silicates in anhydrous CP IDPs and in comet spectra indicate that the majority of GEMS-like materials never saw temperatures above $\sim$1000 K (*Brownlee et al.*, 2005).

Mg-rich amorphous silicates anneal at lower temperatures or in less time than Mg-Fe amorphous silicates, so given a reservoir of Mg-rich and Mg-Fe amorphous silicates, Mg-rich crystalline silicates are more likely an outcome of the primary thermal processing of annealing. However, the transient heating events would have to be just of the right duration to anneal all the Mg-rich amorphous silicates into Mg-rich crystals but not anneal a significant fraction of the Mg-Fe amorphous silicates into Mg-Fe crystalline silicates. Given the improbability of this 'fine-tuning' of transient heating events, we look to combine another physical process – Fe reduction – with annealing to metamorphose Mg-Fe amorphous silicates into Mg-rich crystalline silicates.

3.4 Removal of Fe from Mg-Fe Silicates by Reduction, on Mg-Fe Inter-diffusion Time Scales

Experimental heating of Mg-Fe olivines, typically $(Mg_{0.9},Fe_{0.1})_2SiO_4$, in a reducing environment causes the FeO in the mineral to be reduced to Fe-metal, increasing the Mg-content of the olivine, and in many cases forming Fe-metal blebs on the surface (*Allen et al.*, 1993; *Weisberg et al.*, 1994). In these experiments, O is scavenged from the silicates in a 'locally reducing' environment caused either by a low partial pressure of oxygen or by a 'reducing agent' in contact with the grain surface, such as graphitic C that combusts to CO or CO_2.

Experiments demonstrating Fe-reduction have utilized a wide variety of heating temperatures and sample preparations, including $\sim$20–100 μm-radii powders, bulk minerals, and thin films. Flash-melting ($\geq$1873 K) chondrule-precursor 20–100 μm–radii ground mineral powders mixed with $\geq$5 wt-% C produces from $(Mg_y,Fe_{(1-y)})_2SiO_4$, y=0.94–0.89 nearly pure-Mg olivine $(Mg_{0.99},Fe_{0.01})_2SiO_4$, Fe-metal grains and silica (SiO_2) (*Connolly et al.*, 1994a, b; *Connolly*, 1996). Even though within the furnace the oxygen fugacity is $\log(f\mathrm{O}_2[\mathrm{bar}])$ $\approx$–9.5, the oxygen fugacity in the 'local environment' of the melt is lower, $\log(f\mathrm{O}_2[\mathrm{bar}])$ $\approx$–12. At 1873 K, the canonical solar nebula had $\log(f\mathrm{O}_2[\mathrm{bar}])$=–14.7 (–2.7 dex lower than in the experiment), so Fe-reduction can occur in an 'oxygen-rich' environment compared to the solar nebula.

For Fe reduction to occur in the subsolidus, C must be present on grain surfaces: heating of a bulk sample of Mg-rich olivine $(Mg_{0.90},Fe_{0.1})_2SiO_4$ for 5–48 hr at 1373 K, i.e., at a lower temperature than melts, generates $\log(f\mathrm{O}_2[\mathrm{bar}])$=–13, well below (by more than 4 dex) the equilibrium oxygen fugacity, and causes Fe-metal blebs to form on the surface, as well as a gradient in the Mg^{2+}-Fe^{2+} concentration (less Fe^{2+}) and excess SiO_2 in near-surface region, by the following reaction:

$$\mathrm{Fe_2SiO_{4\,in\ olivine}} + 2\mathrm{C_{graphite}} =$$

$$2\mathrm{Fe_{\,in\ surface\ metal}} + \mathrm{SiO_{2\,in\ silicate}} + 2\mathrm{CO_{in\ gas}}$$

Heating at 1000 K a thin film of Mg-rich amorphous olivine, $(Mg_y,Fe_{(1-y)})_2SiO_4$) with y=0.9, reduces the FeO to 0.002–0.05 μm Fe-metal within the amorphous olivine and generates domains of 0.05–0.25 μm size pure-Mg crystalline olivine (Mg_2SiO_4) (*Davoisne et al.*, 2006). In summary, under low oxygen fugacity (fO_2) conditions produced on grain surfaces or in the vicinity of grains by the combustion of C into CO and CO_2, Fe reduction can produce embedded nano-phase or surface Fe-metal grains. Under solar nebula conditions S is available in the gas-phase, so in conjunction with Fe reduction, $Fe_{1-x}S$ grains may form (*Keller et al.*, 2000). $Fe_{1-x}S$ grains are a component of CP IDPs and GEMS subgrains (*Keller et al.*, 2005).

Carbon is an abundant component of cometary grain materials, either as elemental C in the form of amorphous carbon or poorly graphitized carbon, or in organic grain

Table 1: Fe Reduction Times for a 1 μm Radius Grain

	$(Mg_{0.5},Fe_{0.5})_2SiO_4$		$(Mg_{0.92},Fe_{0.08})_2SiO_4$	
T(K)	t(sec)	t(hr)	t(sec)	t(hr)
1000	2.3E4	6.4	1.8E6	494
1200	630	0.2	1.6E4	4.4
1400	20	0.006	630	0.2

materials that can be converted to elemental C by heating (*Keller et al.*, 1996). The higher relative abundance of C in cometary materials compared with meteoritic materials, as well as the intimate contact between carbonaceous and siliceous minerals in anhydrous CP IDPs, supports that the plausibility of the scenario that Fe reduction occurred in the solar nebula, fueled by abundant C in primitive grains (*Sections* 2.2, 2.3).

Can Fe-reduction be efficient enough to explain the absence of Mg-Fe silicate crystals in cometary grains? The rate of Fe reduction appears to be governed by the Mg^{2+}–Fe^{2+} inter-diffusion rates (*Lemelle et al.*, 2001). Fe reduction generates a gradient in the Mg^{2+}–Fe^{2+} concentration because there is less Fe^{+2} beneath the surface where Fe-metal has been reduced on the surface. A 'diffussivity' parameter is derived for Fe reduction that "is close to the diffusivity of Fe^{2+}–Mg^{2+} in olivine" (*Lemelle et al.*, 2001, citing *Nakamura and Schmalzried*, 1984; *Chakraborty*, 1997). Figure 10 shows the inter-diffusion rates for Fe^{2+}–Mg^{2+} (data taken from figures in *Chakraborty*, 1997) and the diffusion rate derived for the Fe reduction to Fe-metal on the surface at 1373 K (*Lemelle et al.*, 2001). Also shown in Fig. 10 is the diffusion rate deduced from the heating of 0.05– 0.1 μm radii GEMS at 1000 K for 'a few hours' (*Brownlee et al.*, 2005), the consequence of which was both the homogenization (complete Mg^{2+}–Fe^{2+} inter-diffusion) and the annealing to a 'moderately Fe-rich' (denoted herein Mg-Fe) crystalline olivine. The lower the concentration of Fe, the longer the diffusion time and longer the reduction time.

From the inter-diffusion rates (Fig. 10), we compute the Fe reduction times for a 0.1 μm-radii grain, the typical size of a monomer within an aggregate CP IDP (Table 1). Diffusion is a 'random walk' process, so $t(\mathrm{sec}) = a(\mathrm{cm})^2/\mathbf{D}(\mathrm{cm}^2\,\mathrm{sec}^{-1})$. At 1200 K, the time scales for Fe reduction of a 0.1 μm-radii $(Mg_{0.5},Fe_{0.5})_2SiO_4$ (Fo50) crystal is about 0.2 hr, which is faster than the completion time for annealing for Fe_2SiO_4 (Fo0) (1 hr at 1273 K), slower than for Mg_2SiO_4 (Fo100) (1 hr at 1073 K) (*Brucato et al.*, 2002; see *Wooden et al.*, 2005 for a comparison of annealing times), and slower for GEMS (Brownlee *et al.*, 2005). A better comparison between the Fe reduction times and annealing time must await future experiments on the annealing of amorphous Mg-Fe silicates and GEMS. The best we can infer from the current laboratory data is that Fe reduction may transform submicron Mg-Fe silicates to Mg-rich silicates on time scales similar to or somewhat (maybe up to a factor of 10 times) longer than annealing time scales.

4. GRAIN HEATING AND RADIAL MIXING IN DISKS

The metamorphism of Mg-Fe amorphous silicates into Mg-rich crystalline silicates can occur in the hotter, inner disk on long time scales under conditions of 'Equilibrium + Radial Diffusion' (Fig. 11). Large scale radial transport subsequently is required to transport the crystals out to the colder, icy comet-forming regions. Mid-plane temperatures of 1400–1000 K needed to condense or anneal Mg-rich crystalline silicates only occur out to 2–4 AU at early times in protosolar disk evolution when the mass accretion rates are high (e.g., $10^{-5}M_\odot$ yr$^{-1} \lesssim \dot{M} \lesssim 10^{-6}M_\odot$ yr^{-1}, *Bell et al.*, 2000). In the early ($\lesssim$300,000 yr) collapse, rapid redistribution of angular momentum phase of the protosolar disk, a warm nebula model generates a uniform crystalline mass

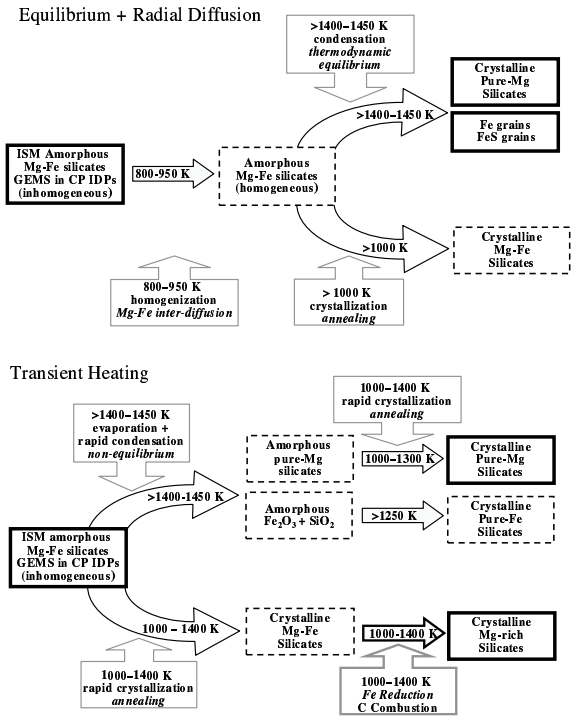

Fig. 11.— Scenarios for the thermal metamorphosis of the silicate mineral complex in protoplanetary disks. **Equilibrium + Radial Transport** in accretion disks provide conditions for thermodynamically-regulated condensation, which converts ISM amorphous Mg-Fe silicates into crystalline pure-Mg silicates and Fe-grains. **Transient Heating** processes, such as in shocks, can (*upper path*) rapidly condense amorphous pure-Mg silicates that can subsequently be annealed into crystalline pure-Mg silicates. **Transient Heating** also can (*lower path*) anneal amorphous Mg-Fe silicates to crystalline Mg-Fe silicates. **Fe Reduction** in the subsolidus phase may remove Fe from crystalline Mg-Fe silicates, transforming them to crystalline Mg-rich silicates. Annealing and Fe reduction can occur at similar temperatures, but Fe reduction may be slower (see *Section* 3.3). In comets and anhydrous CP IDPs, some grain materials are present (*bold borders*) and some are not (*dashed borders*).

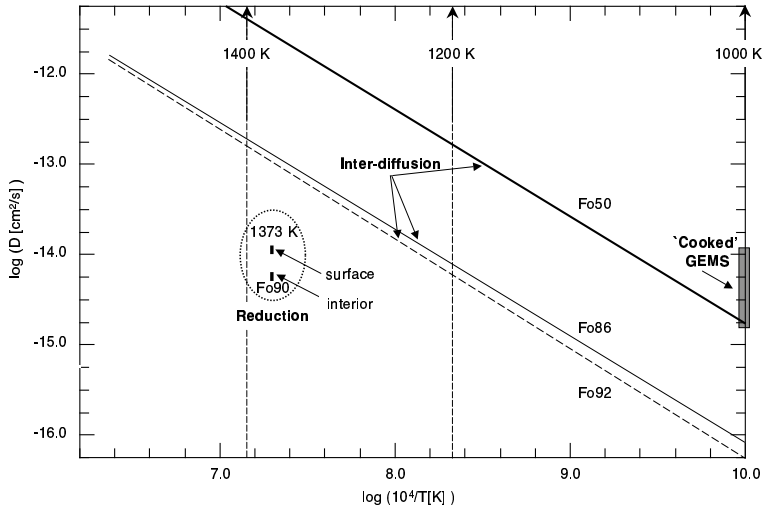

Fig. 10.— Temperature-dependence of diffusion coefficients **D (cm^2 sec^{-1})** for the inter-diffusion of Fe^{2+} with Mg^{2+} (*Chakraborty*, 1997), and for **Fe Reduction** from crystalline olivine (Fo90) at 1373 K. Reduction proceeds at approximately inter-diffusion rates (*Lemelle et al.*, 2001). Fe^{2+} diffuses faster in Mg-Fe (Fo50) compared to Mg-rich (Fo86, Fo92) crystalline olivine.

fraction of $\sim$0.1 throughout the disk (*Bockelée-Morvan et al.*, 2002). A greater fraction of the collapsing mass can be processed through this hotter, inner region of the disk for higher angular momentum cloud cores, yielding a higher uniform crystalline fraction (*Dullemond et al.*, 2006).

In contrast to these uniform crystalline fractions produced in very early stages of disk evolution, models for active disks that incorporate the advection-diffusion-reaction equations can produce radial-gradients in the crystalline fractions (f_{cryst}). Even as the accretion rates decline with time, f_{cryst} spreads to the outer disk regions. These models for actively accreting disks produce radial gradients in the silicate crystalline fraction, with values of a few tens of percent at $\sim$5 AU (*Section* 4.1). These values of f_{cryst} are at most factors of a few lower than the range determined for Oort cloud comets (*Section* 2.3): methods to assess f_{cryst} use the mass of submicron silicate crystals, but may use the mass of only submicron amorphous silicates or the mass of submicron- to 10 μm-radii amorphous silicates, deriving $f_{cryst}\sim$0.6–0.8 or $f_{cryst}\sim$0.4, respectively, from the same IR spectra. A model that uses non-spherical particles, submicron crystals, and submicron- to 100 μm-radii amorphous silicates derives a comparitively very low crystalline fraction of f_{cryst} $\sim$0.075 (*Section* 2.3; *Min et al.*, 2005).

Mg-rich crystals may form by 'transient heating' events such as shocks. Larger volumes of the disk are at lower temperatures, so annealing mechanisms ($\gtrsim$1000 K) can act over larger volumes than can evaporation and condensation ($\gtrsim$1400 K). As the mass accretion rates decline as the disks evolve with time, annealing can continue to act at disk radii where temperatures are too low for evaporation-condensation. Transient heating events include shocks, X-ray flares, and temperature increases arising from increases in opacity, such as may occur when inwardly migrating planetesimals evaporate and increase the dust-to-gas ratio (*Cuzzi et al.*, 2003). At larger disk radii, shocks may not require large scale radial transport (depending on the number of shocks and the shock speeds) to deliver Mg-rich crystals to comet-forming zones (*Section* 4.2). To produce Mg-rich crystals by annealing, transient heating events need to remove Fe, possibly via Fe reduction (Fig. 11), from the Mg-Fe amorphous silicate grains (*Sections* 3.1, 3.3).

Both Deep Impact Mission results (*Section* 2.3) and recent observations of Herbig Ae/Be stars with the MIDI 10 μm interferrometric instrument indicate radial-dependent crystalline fractions exist in protoplanetary disks. MIDI observations show crystalline fractions are enhanced in inner disks by factors of 2–6 (*van Boekel et al.*, 2004). Similar enhancements in the inner disk crystalline fraction are deduced from χ^2-fits of passive disk models to observed Herbig Ae/Be star SEDs (*Harker et al.*, 2005a). Both 'Equilibrium + Radial Diffusion' and 'Transient Heating' models for the formation of Mg-rich crystals out of the initial reservoir of Mg-Fe amorphous silicates need to work towards producing the silicate crystalline fractions provided by observations of comets and external protoplanetary disks.

4.1 Crystalline Radial Gradients in Accretion Disks

In recent time-dependent 2-dimensional (2D) models for the mineralogical evolution of grains in active accretion disks (*Gail*, 2001; *Gail*, 2004; *Wehrstedt and Gail*, 2006), mass accretion carries amorphous Mg-Fe silicate grains into the warm inner disk zones where high temperature equilibrium processes, e.g., homogenization, Mg-Fe diffusion, annealing, and vaporization followed by condensation (*Gail*, 2004), convert the Mg-Fe amorphous silicates, which are non-equilibrium mixtures, into a chemical equilibrium mixture of Fe-grains and Mg-rich crystalline silicates. The

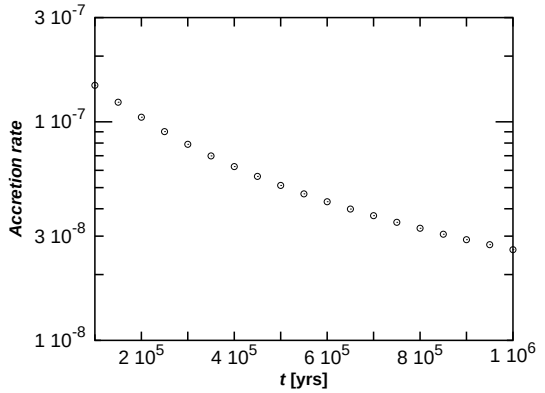

Fig. 12.— Time-dependence of the mass accretion rate in 2-D active disk models (*Wehrstedt and Gail*, 2006).

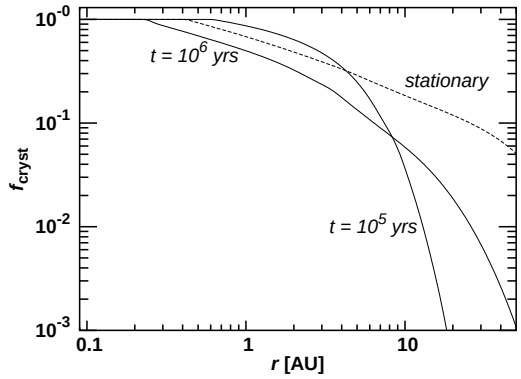

Fig. 13.— From time dependent 2-D models, the radial-dependence of the crystalline olivine fraction (f_{cryst}) at t=10^5 and 10^6 yrs (*Wehrstedt and Gail*, 2006). A stationary model (*Gail*, 2004) with an accretion rate of $3 \times 10^{-8} M_{\odot} yr^{-1}$ over estimates (f_{cryst}) at r>10 AU.

Mg-rich crystals are then mixed outwards by radial transport mechanisms including turbulent diffusion and large-scale circulation currents. The mass accretion rate follows a somewhat rapid decline (Fig. 12), yielding a mass accretion rate of $3 \times 10^{-8} M_{\odot} yr^{-1}$ at a disk age of $t = 10^6$ yr, for the initial set of disk parameters (e.g., angular momentum and initial mass) (*Wehrstedt and Gail*, 2006). The fraction of all olivines that have been transformed by time t to Mg-rich crystalline olivine is shown in Fig 13. In the time dependent 2D model, the radial-dependences of the crystalline fractions for olivines and pyroxenes practically are equivalent (Table 2 in *Wehrstedt and Gail*, 2006). Specifically, in the 2D disk model, at 5 AU the crystalline fraction f_{cryst} evolves from ∼0.3 to 0.1 between 10^5 and 10^6 yr. These theoretical results, thus, suggest models for a less rapidly evolving protosolar disk will produce higher silicate crystalline fractions in the comet-forming zones (*Section* 2.3).

Model calculations based on stationary one-zone α-disks for the dust evolution (*Gail*, 2004), however, over estimate the crystalline fraction (f_{crys}) at >20 AU because mixing cannot transport matter from the innermost parts of the disk (r<1 AU) significantly beyond 20 AU within 10^6 yrs.

Dust grains contribute significantly to the disk opacity. Changes in opacity due to the metamorphosis of the silicate mineralogy from Mg-Fe amorphous silicates ('Fe-rich' silicates of *Pollack et al.*, 1994) to Mg-rich crystalline silicates, however, only moderately impacts the vertical optical depth and the disk's vertical structure (Fig. 6 of *Gail*, 2004).

4.2 Transient Grain Heating in Shocks

The physics of particle heating in shock waves dictates the peak temperature and duration of heating, as discussed and compared in detail in *Desch et al.*, (2005). Several shock mechanisms, advanced as explanations for the melting of chondrules, could create shocks with sufficient speeds to anneal amorphous silicate grains. Accretion shocks with $V_{\rm s} >$ a few $\rm km\,s^{-1}$ are predicted in the vicinity of a proto-Jovian nebula (*Nelson and Ruffert*, 2005), which may anneal grains in the 5–10 AU region where Oort-cloud comets form. Gravitational instabilities in a disk with mass $\sim 0.1\,M_{\odot}$ are predicted to generate shocks with speeds up to $\sim 10\,\rm km\,s^{-1}$, throughout the disk (*Boss and Durisen*, 2005). Annealing by shocks could persist as long as the disk is gravitational unstable beyond these typical radii. According to the calculations of *Bell et al.* (1997), this requires only that the mass flux through the protoplanetary disk exceed $\sim 10^{-9}\,M_{\odot}\,\rm yr^{-1}$, a condition that could persist for many Myr in protoplanetary disks (*Gullbring et al.*, 1998). Shock speeds $\sim 5\,\rm km\,s^{-1}$ therefore seem achievable at heliocentric distances less than about 16 AU (where the Keplerian speed is $15\,\rm km\,s^{-1}$) in the protosolar disk.

The fraction of silicate grains that could be processed by shocks is not known, but in principle could be a substantial fraction of all dust interior to the radii at which these shocks occur. It is important to note that shock models for water-rich regions of the nebula suggest the possible *in situ* aqueous alteration of olivine into layer lattice or phyllosilicates (*Ciesla and Cuzzi*, 2005). Phyllosilicates are missing from comet comae (<1% of Montmorillonite in comet Hale-Bopp, *Wooden et al.*, 1999; *Wooden*, 2002) and rare in anhydrous CP IDPs (*Bradley*, 1988; *Flynn et al.*, 2003); this suggests *in situ* aqueous alteration of siliceous grains was not efficient, shocks were not prevalent in the water-rich region, or radial mixing of phyllosilicates out to the comet-forming zone was extremely inefficient. An important aspect of shock scenarios is that once the transient heating has ended, the disk gas and dust must necessarily return to its ambient temperature. The presence of high and low temperature materials in comets implies mixing between shocked and unshocked regions.

Here, an approximation to the physics of the *Connolly and Desch* (2002) model is used to demonstrate Mg-rich amorphous silicate grains can reach temperatures of ∼1200 K for a fraction of a second, and therefore can be annealed (*Harker and Desch*, 2002). We consider a $5\,\rm km\,s^{-1}$ shock incident upon a gas of ambient density ($\rho_{\rm amb} \approx 10^{-10}\,\rm g\,cm^{-3}$). The shock of Mach number

5.4 compresses the H_2 gas a factor of 6. After crossing the shock front, gas is immediately ($\Delta t \ll 1$ ms) slowed to 1/6 of the incident shock speed, gas heated from $T_{\rm gas} \simeq 150\,{\rm K} \longrightarrow 2000\,{\rm K}$). The gas then cools quickly as it collides with and exchanges thermal energy with dust grains; the stopping times for grains of radii a are short, $1.7\,(a/1\,\mu{\rm m})\,{\rm s}$. The grains are heated by frictional heating and by absorbing radiation from other grains in the vicinity, and are cooled by emitting radiation. Because the timescale for radiative equilibrium is so short, the peak temperature is found by balancing heating and cooling:

$$4\pi a^2\,\bar{Q}_{em}\,\sigma T_{\rm dust}^4 = 4\pi a^2\,\bar{Q}_{abs}\,\pi J + 4\pi a^2\,\frac{1}{8}\rho_{\rm d} V_{\rm drift}^3.$$

Here $\bar{Q}_{em}$ is the Planck-average emissivity ($Q_{em}(\lambda) = Q_{abs}(\lambda)$, Fig. 4) of a grain at its peak temperature, $\bar{Q}_{abs}$ is the Planck-average emissivity of the grain at the temperature of the incident radiation field, characterized by the (frequency-integrated) mean intensity J_{grains} of the emission from the surrounding dust, which depends on the local (dust-dominated) opacity. Given the density of the silicate dust grain $\rho_{\rm d} \approx 3\,{\rm g\,cm^{-3}}$, $\{\bar{Q}_{em},\,\bar{Q}_{abs}\}$ for Mg-Fe amorphous pyroxene ($Mg_{0.5}$,$Fe_{0.5}$)SiO_3, and a shock of speed $V_{\rm s} = 5\,{\rm km\,s^{-1}}$, then minimum ambient gas densities of 0.6, 2.0, 4.0, and 5.0×10^{-10} are required for grains of radii a=0.10, 0.25, 0.5, and 1.0 μmto reach 1200 K for $\sim$0.1 sec and $1200 \leq T_{\rm dust} \leq 1150$ K for $\sim$1 sec, sufficient to to anneal amorphous Mg-silicates (SEI, *Hallenbeck et al.*, 1998, 2000; *Brucato et al.*, 1999; *Wooden et al.*, 2005).

For the protosolar disk, these ambient gas densities of $\sim10^{-10}\,{\rm g\,cm^{-3}}$ are typically found at $\sim$1–10 AU, depending on the mass flux and turbulent viscosity parameter α (*Bell et al.*, 1997). For disks around $2\,M_\odot$ Herbig Ae/Be stars, mid-plane gas densities of $\sim10^{-10}\,{\rm g\,cm^{-3}}$ can occur, with a factor of at least 3 uncertainty, at $\sim$1.5 times greater distances than in the protosolar disk. Shocks driven by gravitational instabilities appear capable of annealing submicron silicate grains out to $\sim$10 AU in the Solar System disk, and out to perhaps 20–30 AU in Herbig Ae/Be disks.

The peak grain temperature in the shock depends on the silicate grain mineralogy. Silicate grains are bathed in the radiation field of other grains of approximately the same temperatures, so $\bar{Q}_{em}(a) \approx \bar{Q}_{abs}(a) \propto a\,T_{dust}$, where a is the grain radius. Thus, the peak temperature may be approximated as

$$T_{\rm dust}^4 \simeq \frac{\pi}{\sigma} J_{grains} + \frac{\rho V_{\rm drift}^3}{8\sigma \bar{Q}_{em}}.$$

From this approximate formula one sees that high peak temperatures are achieved by high gas densities, high shock speeds, or *low* wavelength-dependent emissivities ($Q_\lambda(a)$, Fig. 4) at wavelengths near the peak of their absorption/emission ($\approx 3\,\mu{\rm m}$ for $T = 1200\,{\rm K}$), i.e., low $Q_\lambda(a)$ by either their mineralogy or their smaller grain radii a. Our calculated dust temperatures are for amorphous Mg-Fe grains. Since Mg-rich silicates have lower emissivities at near-IR wavelengths than Mg-Fe silicates by a factor of $\sim$30 in the near-IR (Fig. 4; *Dorschner et al.*, 1995), one expects amorphous Mg-rich silicate grains to achieve higher temperatures (by a factor of $\approx 30^{1/4} \simeq 2.3\times$) than amorphous Mg-Fe silicate grains of the same grain radius, although the exact factor of temperature increase is sensitive to the calculated radiation field J_{grains}. At near-IR wavelengths, $\bar{Q}_{em}$ is approximately linearly dependent on grain radius (Fig. 4), so smaller shock velocities are required to heat smaller grains to the same temperatures. Smaller particles also are stopped quicker ($t_{\rm stop} \approx a\rho_{\rm p}/\rho C_s \propto a$) and therefore heated for a shorter time.

While the peak temperatures of 1200–1150 K occur for only $\sim$0.1–1 sec, grain temperatures of $\gtrsim$1000 K are sustained for fractions of an hour (see *Desch et al.*, 2005 for a detailed discussion of the parameters that affect this temperature plateau). If at 1200 K, a 0.1 μm Mg-Fe (Fo_{50}) olivine grain requires 600 sec (10 min) to reduce the Fe out of the grain on diffusion time scales (Table 1), then this grain would have to be exposed to multiple shocks for it to undergo a metamorphosis to a Mg-rich crystal (*Section* 3.3.). *If a plateau of warmer temperatures ($\sim$1000 K) precedes the shock (for $\gtrsim$ hour) and is sustained post-shock (for more than several hours, as suggested by Fig. 1 of Desch* et al., *2005), then annealing at $\sim$1200 K and Fe reduction at $\sim$1000 K could happen in the same shock.*

5. CONCLUSIONS
Constraints on Transient Heating Events Provided by Cometary Grains

Cometary grains contain volatile organics, refractory organics, and refractory mineral species. Studies of anhydrous CP IDPs and *in situ* measurements show that comet grains are intimate mixtures of ISM materials and materials thermally processed in the protosolar disk. Primary thermal processing and radial transport was happening to submicron-size subgrains at the time of growth of aggregate grains, prior to the incorporation into cometary nuclei. Cometary organic materials were the probable precursors of meteoritic organics and best represent solid-phase ISM organic species. Comparisons between organic species in anhydrous CP IDP and primitive carbonaceous meteorites reveals the effects of thermal processsing. Cometary volatile organic grain species produce 'distributed sources' in cometary comae and have such short lifetimes that they only can be studied in comae. The mere survival of these volatile and refractory organics demonstrates that a significant mass of the outer disk was not subjected to the temperatures required to form crystalline silicates ($\gtrsim$1000 K).

Based on the evidence presented here, Mg-rich crystals are (I) gas-phase condensates that formed under 'Equilibrium Conditions' (thermodynamically-controlled conditions) *or* (II) Mg-rich amorphous silicate gas-phase condensates that formed during 'Transient Heating' events (kinetically-controlled conditions) and that were subsequently annealed with $\sim$100% efficiency, *or* (III) Mg-Fe

amorphous silicates that experienced both annealing and Fe reduction (and Mg-Fe inter-diffusion) metamorphosis that removed the Fe from the grains. Mg-Fe amorphous silicates are abundant in cometary materials, while Mg-Fe crystalline silicates are absent. Therefore, the proposed metamorphosis mechanism (III) needs to be either efficient in converting over a sufficiently long time the entire volume of annealed grains or so efficient that it works in shocks.

Once Mg-rich silicates form, the reducing conditions (low oxygen fugacity $\log(fO_2)$) of the solar nebula favor the maintenance of the separation of Fe into Fe-metal or FeS (i.e., Fe not in the silicates), so condensation is a straight forward mechanism to form Mg-rich crystals. Time-dependent 2D models for the protosolar disk under conditions of 'Equilibrium + Radial Diffusion' can produce radial-gradients in the crystalline fraction f_{cryst}. Relatively rapidly evolving 2D disks produce a crystalline fraction at $\sim$5 AU of $f_{crys} \approx 0.3$ in 10^5 yr, which declines at $\sim$5 AU to $f_{cryst} \approx 0.1$ at 10^6 yr while increasing f_{cryst} at larger radii (*Section* 4.1). These f_{cryst} are near or a factor of a few lower than the crystalline fraction deduced for the submicron portion of the comae grain populations of Oort cloud comets (see *Section* 2.3 for caveats in computing the crystalline fraction using different grain size distributions).

Mass accretion rate decline with time, shrinking the regimes of the disk that are hot enough for condensation and annealing. Therefore, it is advantageous to consider the effects that 'Transient Heating' events such as shocks can have on the production of Mg-rich crystalline silicates.

Shocks are likely to occur in protoplanetary disks (*Section* 4.2). At 5–10 AU, shock speeds produce dust temperatures insufficient to melt dust grains but sufficient to anneal Mg-rich amorphous silicates into Mg-rich crystals. Grains that are shock-heated may be exposed to a peak shock temperature of $\sim$1150–1200 K for 0.1–1 sec and a plateau of higher temperatures of $\sim$1000 K for 0.3–1 hr before and for $\sim$several hours post-shock. Therefore, Fe reduction at $\sim$1000 K concurrent with annealing is a possible mechanism for the metamorphosis of Mg-Fe silicates to Mg-rich silicates during transient heating events in the solar nebula.

Fe reduction is facilitated by the relatively high carbon abundances in cometary grains, including the amorphous carbon or poorly graphitized carbon and organic materials that appear to be the 'glue' that holds together the refractory mineral subgrains, primarily ($\gtrsim$70% by mass, *Section* 2.3) Mg-Fe amorphous silicates. When carbon is in contact with silicate mineral grain surfaces, the combustion of C into CO and CO_2 produces an even lower 'local' oxygen fugacity so that Fe reduction can occur in the subsolidus, forming embedded nanophase Fe or Fe-metal blebs on grain surfaces. For submicron-radii grains, Fe reduction can occur in ten minutes to $\sim$six hours at temperatures of 1200–1000 K. Annealing occurs at these time scales or faster, depending on the Mg-content of the initial amorphous silicate material.

Annealing plus Fe reduction implies the presence of crystalline Mg-rich silicates, e.g., Fo90–Fo75, whereas chemical equilibrium implies crystalline pure-Mg silicates, e.g., Fo100. Mg-rich and pure-Mg crystalline silicates are found in anhydrous CP IDPs (*Section* 2.3), and a census of their relative mass fractions is a subject of current research on anhydrous CP IDPs.

In conclusion, an efficient mechanism for the metamorphosis of Mg-Fe amorphous silicates to Mg-rich amorphous silicates is needed for annealing scenarios to succeed and for shock-annealing scenarios to prevail. Furthermore, large-scale radial transport of crystalline grains is required by scenarios (I) and (II), while it may not be for scenario (III). Future models of radial transport will contribute to our assessment of how far, at what rate, and over what time scales different radial transport mechanisms can act.

Acknowledgments. We thank the referee Ed Scott for his thoughtful comments, and Harold Connolly for discussions on Fe reduction. This work was partially supported by NASA Solar Systems Origins (RTOP 344-37-21-03) and NASA Planetary Astronomy (RTOP 344-32-21-04) (DHW, DEH), and by the National Science Foundation (AST-03-07466) (DEH).

REFERENCES

A'Hearn M. F., Belton M. J. S., Delamere W. A., Kissel J., Klaasen K. P., *et al.* (2005) *Science, 310*, 258-264.

Allen C. C., Morris R. V., Lauer H. V. Jr., and McKay D. S. (1993) *Icarus, 104*, 291-300.

Bell K. R., Cassen, P. M., Klahr H. H., and Henning T. (1997) *Astrophys. J., 486*, 372-387.

Bell K. R., Cassen, P. M., Wasson, J. T., and Woolum, D. S. (2000) In *Protostars and Planets IV* (V. Mannings, *et al.*, eds.), pp. 897-926. Univ. of Arizona, Tucson.

Bockelée-Morvan D. and Crovisier J. (2002) *Earth, Moon, and Planets*, *89*, 5371.

Bockelée-Morvan D., Brooke T. Y., and Crovisier J. (1995) *Icarus*, 116, 18

Bockelée-Morvan D., Lis D. C., Wink J. E., Despois D., Crovisier J., *et al.* (2000), *Astron. Astrophys., 353*, 1101-1114.

Bockelée-Morvan D., Gautier D., Hersant F., Huré J.-M., and Robert, F. (2002) *Astron. Astrophys., 384*, 1107-1118.

Bockelée-Morvan D., Crovisier J., Mumma M. J., and Weaver H. A. (2004) In *Comets II* (M. Festou, *et al.*, eds.) pp. 391-423. Univ. of Arizona, Tucson.

Boss A. P. and Durisen R. H. (2005) *Astrophys. J., 621*, L137-L140.

Bouwman J., Meeus G., de Koter A., Hony S., Dominik C., and Waters L. B. F. M. (2001) *Astron. Astrophys., 375*, 950-962.

Bouwman J., de Koter, A., Dominik C., and Waters L. B. F. M. (2003) *Astron. Astrophys., 401*, 577-592.

Bradley J. P. (1988) *Geochim. Cosmochim. Acta, 52*, 889-900.

Bradley J. P. (1994a) *Science, 265*, 925-929.

Bradley J. P. (1994b) *Geochim. Cosmochim. Acta, 58*, 2123-2134.

Bradley J. P., Brownlee D. E., and Veblen D. R. (1983) *Nature, 301*, 473-477.

Bradley J. P., Humecki H. J., and Germani M. S. (1992) *Astrophys. J., 394*, 643-651.

Bradley J. P., Keller L. P., Gezo J., Snow T., Flynn G. J., Brownlee, and D. E., Bowey J. (1999a) *Lunar Planet. Sci., 30*, 1835.

Bradley J. P., Snow T. P., Brownlee D. E., and Hanner M. S. (1999b) In *Solid Interstellar Matter: The ISO Revolution* (L. d'Hendecourt C. Joblin, and A. Jones, eds.), pp. 297-315. EDP Sciences and Springer-Verlag, Les Houches.

Bradley J. P., Keller L. P., Snow T. P., Hanner M. S., Flynn G. J., *et al.* (1999c) *Science*, *285*, 1716-1718.

Brearley A. J. (1989) *Geochim. Cosmochim. Acta*, *53*, 2395-2411.

Brownlee D. E., Joswiak D. J., Schlutter D. J., Pepin R. O., Bradley J. P., *et al.* (1995) *Lunar Planet. Sci.*, *26*, 183-184.

Brownlee D. E., Joswiak D. J., and Bradley J. P. (1999) *Lunar Planet. Sci.*, *30*, 2031.

Brownlee D. E., Joswiak D. J., Bradley J. P., Matrajt G., and Wooden D. H. (2005) *Lunar Planet. Sci.*, *36*, 2391.

Brucato J. R., Colangeli L., Mennella V., Palumbo P., and Bussoletti E. (1999) *Astron. Astrophys.*, *348*, 1012-1019.

Brucato J. R., Mennella V., Colangeli L., Rotundi A., and Palumbo P. (2002) *Planet. Space Sci.*, *50*, 829-837.

Brucato J. R., Strazzula G., Baratta G., and Colangeli L. (2004) *Astron. Astrophys.*, *413*, 395-401.

Campins H., and Ryan E. (1989) *Astrophys. J.*, *341*, 1059-1066.

Carrez P., Demyk K., Cordier P., Gengembre L., Grimblot J., d'Hendecourt L., Jones A. P., and Lerouz H. (2002) *Meteorit. Planet. Sci.*, *37*, 1599-1614.

Chakraborty S. (1997) *J. Geophys. Res.*, *102*, 12317-12332.

Chihara H., Koike C., Tsuchiyama A., Tachibana S., and Sakamoto D. (2002) *Astron. Astrophys.*, *391*, 267-273.

Ciesla F. J. and Cuzzi J. N. (2005) *Lunar Planet. Sci.*, *36*, 1479.

Colangeli L., Mennella V., Di Marino C., Rotundi A., and Bussoletti E. (1995) *Astron. Astrophys.*, *293*, 927-934.

Colangeli L., Henning Th., Brucato J. R., Clément D., Fabian D., *et al.* (2003) *Astron. Astrophys. Rev.*, *11*, 97-152.

Connolly H. C. Jr. (1996) *Meteorit. Planet. Sci.*, *31*, A30-A31.

Connolly H. C. Jr. and Desch S. J. (2002) *Chemie Der Erde*, *64*, 95-125.

Connolly H. C., Jr, Hewins R. H., Ash R. D., Zanda B., Lofgren G. E., and Bourot-Denise M. (1994a) *Nature*, *371*, 136-139.

Connolly H. C., Jr,, Hewins R. H., Ash R. D., Lofgren G. E., Zanda B. (1994b) *Lunar Planet. Sci.*, *25*, 279-280.

Crovisier J., Leech K., Bockelée-Morvan D., Brooke T. Y., Hanner M. S., *et al.* (1997) *Science*, *275*, 1904-1907.

Cuzzi J. N., Davis S. S., and Dobrovolskis A. R. (2003) *Icarus*, *166*, 385-402.

Davies J. K., Roush T. L., Cruikshank D. P., Bartholomew M. J., Geballe T. R., *et al.* (1997) *Icarus*, *127*, 238-245.

Davoisne C., Djouadi Z., Leroux H., d'Hendecourt L., Jones A., and Debouffle D. (2006) *Astron. Astrophys.*, accepted.

Desch S. J., Ciesla F. J., Hood L. L., and Nakamoto T. (2005) In *Chondrites and the Protoplanetary Disk* (A. N. Krot, *et al.*, eds.), pp. 849-872. ASP, San Francisco.

Desch S. J. and Connolly H. C. (2002) *Meteorit. Planet. Sci.*, *37*, 183-207.

DiSanti M. A., Mumma M. J., Dello Russo N., and Magee-Sauer K. (2001) *Icarus*, *153*, 361-390.

Dorschner J., Begemann B., Henning T., Jaeger C., and Mutschke H. (1995) *Astron. Astrophys.*, *300*, 503-520.

Dukes C., Baragiola R., and McFadden L. (1999) *J. Geophys. Res.*, *104*, 1865-1872.

Dullemond C. P., Apai D., and Walch S. (2006) *Astrophys. J.*, accepted.

Ehrenfreund P. and Charnley S. B. (2000) *Ann. Rev. Astron. Astrophys.*, *38*, 427-483.

Ehrenfreund P., Charnley S. B., and Wooden D. H. (2004) In *Comets II* (M. Festou, *et al.*, eds.) pp. 115-133. Univ. of Arizona, Tucson.

Fabian D., Jäger C., Henning T., Dorschner J., and Mutschke H. (2000) *Astron. Astrophys.*, *364*, 282-292.

Flynn G. J., Keller L. P., Feser M., Wirick S., and Jacobsen C. (2003) *Geochim. Cosmochim. Acta*, *67*, 4719-4806.

Flynn G. J., Keller L. P., Jacobsen C., and Wirick S. (2004) *Adv. Space Res.*, *33*, 57-66.

Fomenkova M. N., Chang S., and Mukhin L. M. (1994) *Geochim. Cosmochim. Acta*, *58*, 4503-4512.

Fomenkova M. N. (1999) *Space Sci. Rev.*, *90*, *Issue 1/2*, 109-114.

Furlan E., Calvet N., D'Alessio P., Hartmann L., Forrest W. J., Watson D. M., *et al.* (2005) *Astrophys. J.*, *621*, L129-L132.

Gail H.-P. (2001) *Astron. Astrophys.*, *378*, 192-213.

Gail H.-P. (2003) In *Astromineralogy. Lecture Notes in Physics, Vol. 309.* (T. K. Henning, ed.), pp. 55-120. Springer, Berlin.

Gail H.-P. (2004) *Astron. Astrophys.*, *413*, 571-591.

Gail H.-P. and Sedlmayr E. (1999) *Astron. Astrophys.*, *347*, 594-616.

Gomes R. S. (2003) *Icarus*, *161*, 404-418.

Grossman L. 1972, *Geochim. Cosmochim. Acta*, *38*, 47-64.

Gullbring E., Hartmann L., Briceno C., and Calvet N. (1998) *Astrophys. J.*, *492*, 323-341.

Hallenbeck S. L., Nuth J. A., and Daukantas P. L. (1998) *Icarus*, *131*, 198-209.

Hallenbeck S. L., Nuth J. A., and Nelson R. N. (2000) *Astrophys. J.*, *535*, 247-255.

Hanner M. S. (1999) *Space Sci. Rev.* , *90*, 99-108.

Hanner M. S., and Bradley J. P. (2004) In *Comets II* (M. Festou, *et al.*, eds.) pp. 555-564. Univ. of Arizona, Tucson.

Hanner M. S., Lynch D. K., and Russell R. W. (1994) *Astrophys. J.*, *425*, 274-285.

Harker D. E. and Desch S. (2002) *Astrophys. J.*, *565*, L109-L112.

Harker D. E., Wooden D. H., Woodward C. E., and Lisse C. M. (2002) *Astrophys. J.*, *580*, 579-597.

Harker D. E., Wooden D. H., Woodward C. E., and Lisse C. M. (2004) *Astrophys. J.*, *615*, 1081.

Harker D. E., Woodward C. E., Wooden D. H., and Temi P. (2005a) *Astrophys. J.*, *622*, 430-439.

Harker D. E., Woodward C. E., and Wooden D. H. (2005b) *Science*, *310* 278-280.

Honda M., Kataza H., Okamota Y.K., Miyata T., Yamashita T., Sako S., et. al. (2004) *Astrophys. J.*, *585*, L59-L63.

Jäger C., Fabian D., Schrempel F., Dorschner J., Henning, Th., and Wesch W. (2003) *Astron. Astrophys.*, *401*, 57-65.

Jessberger E. K., Stephan T., Rost D., Arndt P., Maetz M., *et al.* (2001) In *Interplanetary Dust* (E. Grün *et al.*, eds.), pp. 253-294. Springer-Verlag, Berlin.

Jones A. P. (2000) *J. Geophys. Res.*, *105*, 10257-10268.

Joswiak D. J., Brownlee D. E., Bradley J. P., Schlutter D. J., and Pepin R. O. (1996) *Lunar Planet. Sci.*, *27*, 625-626.

Kawakita H., Watanabe J., Ootsubo T., Nakamura R., Fuse T., *et al.* (2004b) *Astrophys. J.*, *601*, L191-L194.

Kawakita H., Watanabe J., Furusho R., Fuse T., Capria M. T., and De Sanctis M. C. (2004a) *Astrophys. J.*, *601*, 1152-1158.

Keller, Ch. and Gail H.-P. (2004) *Astron. Astrophys.*, *415*, 1177-1185.

Keller L. P. and Flynn G. J. (2003) In *Cometary Dust in Astrophysics*, *Abs. No.* 6053. *Lunar Planet. Inst. Contrib. No. 1184.* Lunar Planet. Inst., Houston.

Keller L. P. and Messenger S. (2004a) *Lunar Planet. Sci.*, *35*, 1985.

Keller L. P. and Messenger S. (2004b) *Meteorit. Planet. Sci., 39*, 5186.

Keller L. P., and Messenger S. (2005) In *PPV Poster Proceedings* http://www.lpi.usra.edu/meetings/ppv2005/pdf/8570.pdf

Keller L. P., Thomas K. L., and McKay D. S. (1996) In *Physics, Chemistry, and Dynamics of Interplanetary Dust. ASP Conf. Ser. 104* (B. A. S. Gustafson and M. S. Hanner, eds.), pp. 295-298. ASP, San Francisco.

Keller L. P., Messenger S., and Bradley J. P. (2000) *J. Geophys. Res., 105, A5*, 10397-10402.

Keller L. P., Messenger S., Flynn G. J., Clemett S., Wirick S., and Jacobsen C. (2004) *Geochim. Cosmochim. Acta, 68*, 2577-2589.

Keller L. P., Messenger, S., and Christoffersen R. (2005) *Lunar Planet. Sci., 36*, 2088.

Kemper F., Waters L. B. F. M., de Koter A., Tielens A. G. G. M. (2001) *Astron. Astrophys., 369*, 132-141

Kemper F., Vriend, W. J., and Tielens A. G. G. M. (2004) *Astrophys. J.*, 609, 826-837.

Kemper F., Vriend, W. J., and Tielens A. G. G. M. (2005) *Astrophys. J., 633*, 534-534.

Kenyon S. J., Hartmann L. W., and Kolotilov E. A. (1991) *Publ. Astron. Soc. Pac. , 103*, 1069-1076.

Kerridge J. F. (1999) *Space Sci. Rev., 90*, 275-288.

Khare B. N., Thompson W. R., Sagan C., Arakawa E. T., Meisse C., and Gilmour I. (1990) *Lunar Planet. Sci. , 21*, 627.

Kimura H., Kolokolova L., and Mann I. (2003) *Astron. Astrophys., 407*, L5-L8.

Kissel J. (1999) In *Formulation and Evolution of Solids in Space* (J. M. Greenberg and A. Li, eds.), pp. 427-445. Kluwer, Dordrecht.

Koike C., Chihara H., Tsuchiyzma A., Suto H., Sogawa H., and Okuda H. (2003) *Astron. Astrophys., 399*, 1101-1107.

Lemelle L., Guyot F., Leroux H., and Libourel G. (2001) *Amer. Min., 86*, 47-54.

Li A. and Draine B. T. (2001) *Astrophys. J., 550*, L213-L216.

Mann I., Czechowski A., Kimura H., Köhler M., Minato T., and Yamamoto T. (2005) In *IAU Symp. 229, Asteroids, Comets, and Meteors*, in press. Cambridge U. Press, Cambridge.

Messenger S. (2000) *Nature, 404*, Issue 6781, 968-971.

Messenger S., Walker R. M., Clemett S. J., and Zare R. N. (1996) *Lunar Planet. Sci., 27*, 867-868.

Messenger S., Keller L. P., Stadermann F. J., Walker R. M., and Zinner E. (2003) *Science, 300*, 105-108.

Min M., Hovenier J. W., de Koter A., Waters L. B. F. M., and Domonik C. (2005) *Icarus, 179*, 158-173.

Min M., Waters L. B. F. M., Hovenier J. W., de Koter A., Keller L. P., and Markwick-Kemper F. (2005), In *PPV Poster Proceedings* http://www.lpi.usra.edu/meetings/ppv2005/pdf/8478.pdf

Molster F. J. and Kemper, C. (2005) *Space Sci. Rev. , 119*, 3-28.

Molster F. J., Bradley J. P., Sitko M. L., and Nuth J. A. (2001) *Lunar Planet. Sci., 32*, 1391.

Molster F. J., Demyk A., d'Hendecourt L., Bradley J. P., Bonal L., and Borg J. (2003) *Lunar Planet. Sci., 34*, 1148.

Morbidelli A. and Levison H. F. (2003) *Nature, 422*, 30-31.

Nakamura A. and Schmalzried H. (1984) *Berichte der Bunsengesellschaft für Physikalische Chemie, 88*, 140-145.

Nelson A. F. and Ruffert M. (2005) In *Chondrites and the Protoplanetary Disk* (A. N. Krot, *et al.*, eds.), pp. 903-914. ASP, San Francisco

Nier A. O. and Schlutter D. J. (1993) *Meteoritics, 28*, 412-461.

Nuth J. A. and Johnson N. M. (2006) *Icarus, 180*, 243-250.

Nuth J. A., III, Rietmeijer J. M., and Hill H. G. M. (2002) *Meteorit. Planet. Sci. , 37*, 1579

Nuth J. A. III, Brearley A. J., Scott E. R. D. (2005) In *Chondrites and the Protoplanetary Disk* (A. N. Krot, *et al.*, eds.), pp. 675-700. ASP, San Francisco.

Petaev M. I. and Wood J. A. (1998) *Meteorit. Planet. Sci., 33*, 1123

Petaev M. I. and Wood J. A. (2005) In *Chondrites and the Protoplanetary Disk* (A. N. Krot, *et al.*, eds.), pp. 373-406. ASP, San Francisco.

Pollack J. B., Hollenbach D., Beckwith S., Simoneli D. P., Roush T., and Fong W. (1994) *Astrophys. J., 421*, 615-639.

Rietmeijer F. J. M. (1998) In *Planetary Materials, Rev. in Mineralogy, Vol. 36* (J. J. Papike, ed.), pp. 2-1–2-95. Mineralogical Soc. America, Washington, D. C.

Rietmeijer F. J. M., Hallenbeck S. L., Nuth J. A., and Karner J. M. (2002) *Icarus , 156*, 269-286.

Savage K. R. and Sembach B. D. (1996) *Ann. Rev. Astron. Astrophys., 34*, 279-329.

Schulze H. and Kissel J. (1992) *Meteoritics, 27*, 286-287.

Schulze H., Kissel J., and Jessberger E. K. (1997) In *From Stardust to Planetesimals. ASP Conf. Ser. 122* (Y. J. Pendleton and A. G. G. M. Tielens, eds.), pp. 397-414. ASP, San Francisco.

Scott E. R. D. and Krot A. N. (2005) *Astrophys. J., 623*, 571-578.

Shu F. H., Shang H., Gounelle M., Glassgold A. E., and Lee T. (2001) *Astrophys. J., 548*, 1029-1050.

Spitzer L. Jr. and Jenkins E. B. (1975) *Ann. Rev. Astron. Astrophys., 13*, 133-164.

Sugita S., Ootsubo T., Kadono T., Honda M., Sako S., *et al.* 2005, *Science, 310*, 274-278.

Thomas K. L., Keller L. P., Blanford G. E., and McKay D. S. (1994) In *Analysis of Interplanetary Dust. AIP Conf. Proc. Vol. 310* (M. E. Zolensky, *et al.*, eds.), pp. 165-174. Springer-Verlag, Berlin.

Thomas K. L., Keller L. P., and McKay D. S. (1996) In *Physics, Chemistry, and Dynamics of Interplanetary Dust. ASP Conf. Ser. 104* (B. A. S. Gustafson and M. S. Hanner, eds.), pp. 283-286. ASP, San Francisco.

Thompson S. P., Fonti S., Verrienti C., Blanco A., Orofino V., and Tang C. C. (2002) *Astron. Astrophys., 395*, 705-717.

Thompson S. P., Fonti S., Verrienti C., Blanco A., Orofina V., and Tang C. C. (2003) *Meteorit. Planet. Sci., 38*, 457-478.

Tielens A. G. G. M. (2003) *Science*, 300, 68-70.

van Boekel R., Min M., Leinert, Ch., Waters L. B. F. M., Richichi A., Chesneau O., *et al.* (2004) *Nature, 432*, 479-482.

Wehrstedt M. and Gail H.-P. (2002) *Astron. Astrophys., 385*, 181-204.

Wehrstedt M. and Gail H.-P. (2006) *Astron. Astrophys.*, accepted.

Weisberg M. K., Prinz M., and Fogel R. A. (1994) *Meteoritics , 29*, 362-373.

Wooden D. H. (2002) *Earth, Moon, and Planets*, 89, 247

Wooden D. H., Harker D. H., Woodward C. E., Butner H. M., Koike C., *et al.* (1999) *Astrophys. J., 517*, 1034-1058.

Wooden D. H., Butner H. M., Harker D. E., and Woodward C. E. (2000) *Icarus, 143*, 126-137.

Wooden D. H., Woodward C. E., and Harker D. E. (2004) *Astrophys. J., 612*, L77-L80.

Wooden D. H., Harker D. E., and Brearley A. J. (2005) In *Chondrites and the Protoplanetary Disk* (A. N. Krot, *et al.*, eds.), pp. 774-810. ASP, San Francisco.